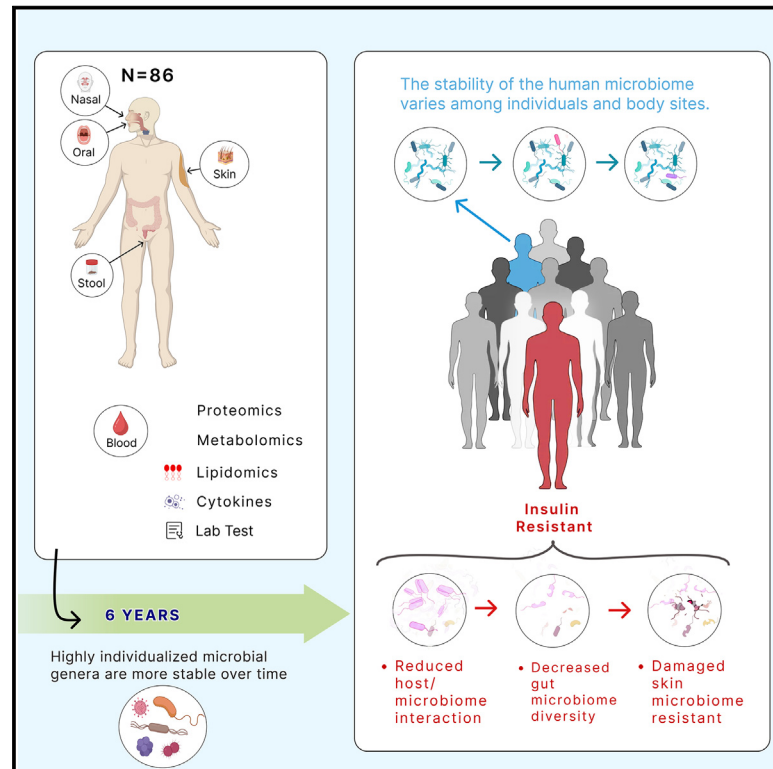


Cell Host & Microbe

Longitudinal profiling of the microbiome at four body sites reveals core stability and individualized dynamics during health and disease

Graphical abstract



Authors

Xin Zhou, Xiaotao Shen, Jethro S. Johnson, ..., Erica Sodergren, George M. Weinstock, Michael P. Snyder

Correspondence

mpsnyder@stanford.edu

In brief

Zhou et al. explore the complex interactions between human microbiomes and their hosts across different body sites, revealing that microbiome stability and its impact on health are influenced by site-specific host factors. Their findings underscore the systemic nature of host-microbiome relationships, with significant implications for understanding metabolic diseases.

Highlights

- The stability of the human microbiome varies among individuals and body sites
- Highly individualized microbial genera are more stable over time
- At each body site, coordinated microbial dynamics are observed in response to disease
- Microbiome stability and skin microbial composition are altered with insulin resistance

Article

Longitudinal profiling of the microbiome at four body sites reveals core stability and individualized dynamics during health and disease

Xin Zhou,^{1,2,3,4,17} Xiaotao Shen,^{1,2,17} Jethro S. Johnson,^{4,5} Daniel J. Spakowicz,^{4,6} Melissa Agnello,⁷ Wenyu Zhou,^{1,2} Monica Avina,¹ Alexander Honkala,^{1,8,9} Faye Chleilat,¹ Shirley Jingyi Chen,⁸ Kexin Cha,⁸ Shana Leopold,^{4,10} Chenchen Zhu,¹ Lei Chen,^{4,11} Lin Lyu,¹¹ Daniel Hornburg,¹ Si Wu,¹ Xinyue Zhang,¹ Chao Jiang,^{1,12} Liuyiqi Jiang,¹² Lihua Jiang,¹ Ruiqi Jian,¹ Andrew W. Brooks,¹ Meng Wang,¹ Kevin Contrepois,¹ Peng Gao,¹ Sophia Miryam Schüssler-Fiorenza Rose,¹ Thi Dong Binh Tran,⁴ Hoan Nguyen,⁴ Alessandra Celli,¹ Bo-Young Hong,^{4,13} Eddy J. Bautista,^{4,14} Yair Dorsett,^{4,15} Paula B. Kavathas,^{10,16} Yanjiao Zhou,^{4,15} Erica Sodergren,⁴ George M. Weinstock,⁴ and Michael P. Snyder^{1,2,3,8,18,*}

¹Department of Genetics, Stanford University School of Medicine, Stanford, CA 94305, USA

²Stanford Center for Genomics and Personalized Medicine, Stanford, CA 94305, USA

³Stanford Diabetes Research Center, Stanford, CA 94305, USA

⁴The Jackson Laboratory for Genomic Medicine, Farmington, CT 06032, USA

⁵Oxford Centre for Microbiome Studies, Kennedy Institute of Rheumatology, University of Oxford, Roosevelt Drive, Headington, Oxford OX3 7FY, UK

⁶Division of Medical Oncology, Ohio State University Wexner Medical Center, James Cancer Hospital and Solove Research Institute, Columbus, OH 43210, USA

⁷Medical Affairs, uBiome, San Francisco, CA 94103, USA

⁸Stanford Healthcare Innovation Labs, Stanford University School of Medicine, Stanford, CA 94305, USA

⁹Department of Biomedical Engineering, Oregon Health & Science University, Portland, OR 97239, USA

¹⁰Department of Immunobiology, Yale University School of Medicine, New Haven, CT 06520, USA

¹¹Shanghai Institute of Immunology, Shanghai Jiao Tong University, Shanghai 200240, PRC

¹²Life Sciences Institute, Zhejiang University, Hangzhou, Zhejiang 310058, PRC

¹³Woody L Hunt School of Dental Medicine, Texas Tech University Health Science Center, El Paso, TX 79905, USA

¹⁴Corporación Colombiana de Investigación Agropecuaria (Agrosavia), Headquarters-Mosquera, Cundinamarca 250047, Colombia

¹⁵Department of Medicine, University of Connecticut Health Center, Farmington, CT 06032, USA

¹⁶Department of Laboratory Medicine, Yale University School of Medicine, New Haven, CT 06520, USA

¹⁷These authors contributed equally

¹⁸Lead contact

*Correspondence: mposnyder@stanford.edu

<https://doi.org/10.1016/j.chom.2024.02.012>

SUMMARY

To understand the dynamic interplay between the human microbiome and host during health and disease, we analyzed the microbial composition, temporal dynamics, and associations with host multi-omics, immune, and clinical markers of microbiomes from four body sites in 86 participants over 6 years. We found that microbiome stability and individuality are body-site specific and heavily influenced by the host. The stool and oral microbiome are more stable than the skin and nasal microbiomes, possibly due to their interaction with the host and environment. We identify individual-specific and commonly shared bacterial taxa, with individualized taxa showing greater stability. Interestingly, microbiome dynamics correlate across body sites, suggesting systemic dynamics influenced by host-microbial-environment interactions. Notably, insulin-resistant individuals show altered microbial stability and associations among microbiome, molecular markers, and clinical features, suggesting their disrupted interaction in metabolic disease. Our study offers comprehensive views of multi-site microbial dynamics and their relationship with host health and disease.

INTRODUCTION

The human microbiome comprises highly dynamic microbial communities inhabiting various body sites,^{1–5} engaging in intricate host-microbial interactions that display territory-specific complexity.^{6–10} Advancements in multi-omics technologies have

catalyzed the elucidation of the molecular mechanisms underlying microbial ecology and their interactions with host, unveiling the critical roles of the microbiome in normal physiological processes such as aging^{11–13} as well as diseases including inflammatory bowel disease (IBD),^{14–16} cardiovascular disease,^{17–19} and type 2 diabetes mellitus (T2DM).^{20–23}

The etiology and pathogenesis of insulin resistance and T2DM have been closely linked to the human microbiome.^{24–27} Patients with impaired insulin and glucose homeostasis exhibit shifted microbiome composition in the gut,^{21,23,25–29} skin,^{30–33} and other body sites,^{34–40} reflecting an ecological dysbiosis characterized by altered microbial alpha diversity,^{25,41} decreased compositional stability,^{42,43} and greater inter-individual variability.²⁵ Compromised mucosal and skin barrier integrity, often associated with insulin resistance, may potentiate microbial translocation, thereby exacerbating systemic inflammation.^{44–47} Although human microbiome studies are often, by necessity, observational, a causal relationship between microbiome dysbiosis and impaired glucose/insulin homeostasis has been demonstrated through human microbiome manipulation.^{41,48,49}

While prior studies on the microbiome and glucose homeostasis have been informative, they exhibit certain limitations. First, these studies^{21,50,51} often lack dense longitudinal sampling, essential for capturing stability features, thus limiting fundamental insights into host-microbe interactions.^{52–54} Second, they primarily focus on the microbiome from a single host site,^{4,50,55–58} overlooking the importance of simultaneous multi-region sampling for assessing microbiome site-specific dynamics, and their interplay across various host microenvironments.^{9,59–62} Lastly, most studies^{8,18,21,63–66} do not concurrently measure host clinical and molecular phenotypes, impeding the exploration of the molecular relationships underpinning health and disease-related host-microbiome interactions.^{67,68}

Collaborative initiatives like the Integrative Human Microbiome Project (iHMP) and Integrative Personal Omics Profiling (iPOP) offer avenues to surmount previous studies' limitations by investigating well-characterized human longitudinal cohorts.^{69–71} In this study, we examined the relationships between multi-site microbiomes and host health in the context of prediabetes, through characterizing the microbiome collected from four body sites in 86 adults for over 6 years and examining their associations with host omics and clinical characteristics. We describe unique longitudinal trajectories for microbiomes across different body sites, demonstrating their responsiveness to both host-specific and environmental factors. We found that personalized microbiomes exhibit greater stability than communal microbes, highlighting the resilience of the individualized microbiome. Nonetheless, these systems remain vulnerable to disturbances like viral infections, which may precipitate dysbiosis linked to metabolic dysfunctions. Furthermore, our analysis revealed associations between site-specific microbiomes and clinical parameters such as cytokine profiles and insulin sensitivity, highlighting the intertwined nature of immune activity and metabolic well-being.

RESULTS

Description of the study design

We analyzed stool, skin, oral, and nasal microbiome from a human cohort of 86 participants for up to 6 years (1,126.6 ± 455.8 days) (Figure 1A; see STAR Methods). The cohort comprised 41 males and 45 females, aged between 29 and 75 years old (55 ± 9.8 years old), with BMIs ranging from 19.1 to 40.8 kg/m² (28.31 ± 4.44 kg/m²) (Table S1A). Sampling occurred quarterly, with an additional 3–7 samples collected within

5 weeks (12% of the total) during periods of stress, such as respiratory illness, vaccination, or antibiotic use. The 16S ribosomal RNA gene sequencing method employed in this study targeted a variable region to facilitate the detection of amplicon sequence variants (ASVs),⁷² enabling the identification and differentiation of most bacterial taxa at the genus and species levels.^{73,74}

A unique feature of this cohort is the multi-omics phenotyping of participants at each time point (Figure 1B). Untargeted proteomics (302 proteins), untargeted metabolomics (724 annotated metabolic features), targeted lipidomics (846 annotated lipids), and 62 targeted cytokine and growth factor measurements were performed, along with 51 clinical markers, including C-reactive protein (CRP), fasting glucose (FG), hemoglobin A1C (HbA1C), low-density lipoprotein (LDL), and high-density lipoprotein (HDL) from plasma samples (Figure 1A). Glucose control assessments, comprising an annual oral glucose tolerance test for all participants and a gold-standard steady-state plasma glucose (SSPG) measurement⁷⁵ for 58 individuals, classified 28 individuals as insulin sensitive (IS) and 30 as insulin resistant (IR) (Figure 1C). Overall, we analyzed a total of 3,058 visits, 5,432 biological samples (1,467 plasma samples, 926 stool samples, 1,116 skin samples, 1,001 oral samples, and 922 nasal samples) generating a total of 118,124,374 measurements. The microbial and other data can be found on our data portal: <https://portal.hmpdacc.org/>.

Microbial demographics and personalization across body sites: Unraveling the impact of diet and environment

We initially examined the overall demographics of the microbiome at each of the four body sites (Figures 1D and S1A). Extending previous studies,^{7,62,76–78} we observed a separation between body sites, including a clear boundary of the skin and nasal samples, highlighting the pronounced territory specificity of each microbiome.^{6,7,79}

Micro-biotypes, like enterotypes in the stool microbiome,^{50,77,78} are present in all body sites, with their community structure predominantly influenced by specific taxa. The stool microbiome primarily exhibited a gradient of abundance distributions between *Bacteroidetes* and *Firmicutes*, except for a few samples with high *Prevotella*. The recently identified core genus *Phocaeicola*⁸⁰ had minimal impact on the overall *Bacteroidetes/Firmicutes* gradient, but samples with high *Phocaeicola* and *Bacteroides* were clearly separated (Figure S1A). The oral microbiome was primarily composed of *Prevotella*, *Streptococcus*, *Veillonella*, *Haemophilus*, *Neisseria*, and *Leptotrichia*, as previously described.^{81–83} The skin and nasal microbiome samples jointly displayed a triangular distribution, primarily driven by three dominant genera: *Cutibacterium*, *Corynebacterium*, and *Staphylococcus* (Figures 1D and S1A).^{4,8,62,79} The distribution of microbial genera remained consistent with findings from other cohorts,^{8,59,84} irrespective of participant diversity in insulin sensitivity in our study (Figure S1B). Our study, however, extends these observations by longitudinally comparing inter- and intra-individual covariance across all four body sites within the same cohort.

Intraclass (intra-individual) correlation coefficient (ICC) analysis confirmed that microbial personalization is more pronounced at the ASV level than at broader taxonomic resolutions

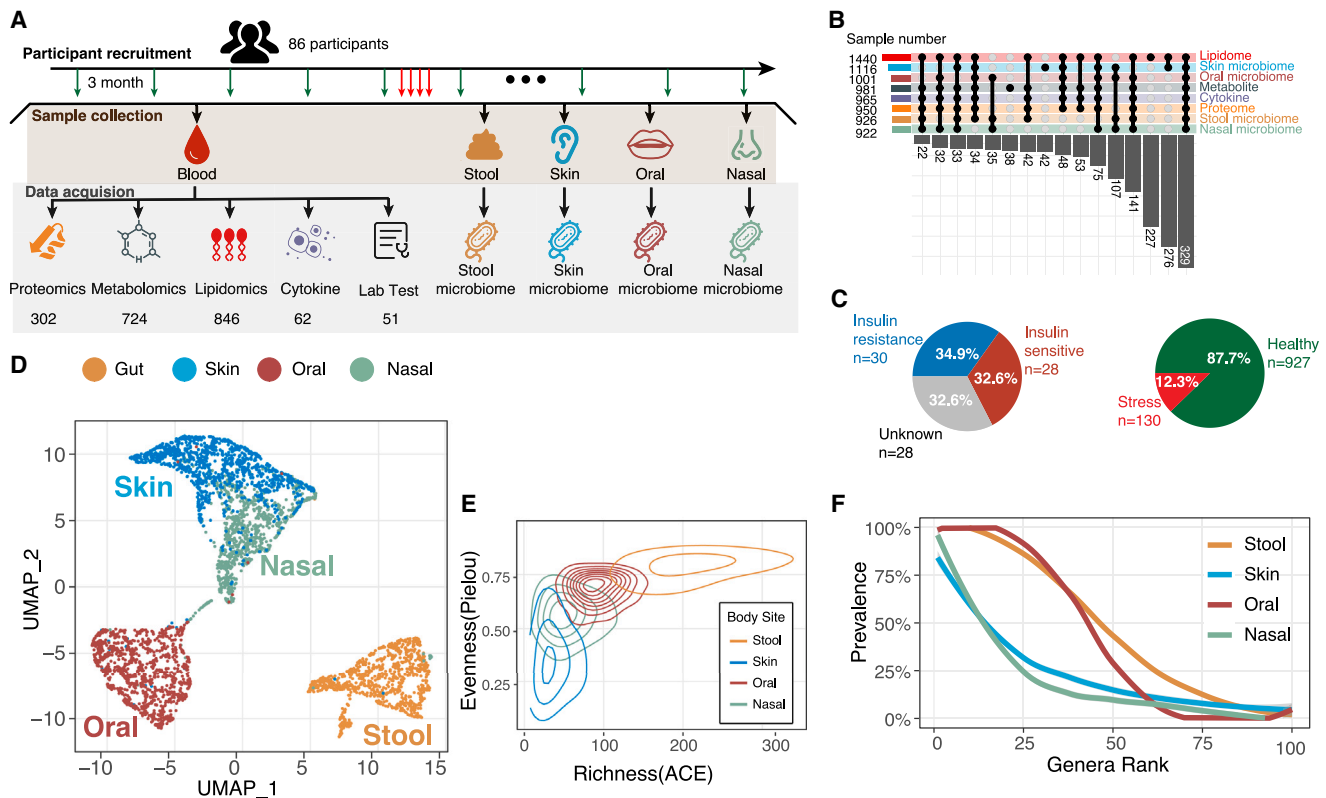


Figure 1. Longitudinal profiles of the microbiome at four body sites

- (A) Study design.
 (B) Overlap of sample numbers among different omics types.
 (C) Proportion of stress, insulin resistant, and healthy samples.
 (D) Uniform manifold approximation and projection (UMAP) of microbiome samples by body site.
 (E) Density distribution of microbiome richness and evenness.
 (F) Rank prevalence curve of microbiome genera with the 100 highest longitudinal prevalence at each body site.

(Figure S1C), highlighting stronger individualization with finer taxonomy resolution. Notably, despite similar ecological characteristics and dominant bacterial constituents, the nasal microbiome manifested greater personalization than the skin microbiome (Figure S1D), presumably because nasal microbiome dynamics are more host dependent.⁷⁹

While environmental factors like season and diet can influence the human microbiome, our results suggest that the impact of seasonality on the gut microbiome, despite mixed results in previous studies,^{50,85–87} is relatively modest. Likely due to its direct external exposure, the skin microbiome exhibited the largest seasonal dynamic. This was followed by the oral microbiome, which may be shaped by seasonal dietary changes,^{51,88,89} as it explained more dietary variance than other sites (Figure S1E). We also observed a significant fluctuation of the skin and oral microbiome evenness: these two communities both become more even during summer with an increased number of different microbes (Figure S1F) possibly triggered by environmental changes such as temperature and humidity.^{85,90} Based on two participants with accessible environmental and chemical exposure data,⁹⁰ we found stronger exposome-skin microbiome covariance than in other body sites (Figure S1G) with noticeable environmental impacts on internal sites like oral and stool micro-

biomes,⁹¹ supporting our earlier single-individual observation.⁹² By modeling⁸⁵ the microbial dynamics across seasons, we found more pronounced alterations in skin and nasal microbiomes than in stool and oral microbiomes (Table S1B). These findings not only extend our knowledge of gut microbiome specificity and individuality^{56,93} to other body sites but also broaden our understanding of environmental influences on microbiomes, with diet shaping oral microbiomes and environmental exposure impacting skin and nasal microbiomes.

Microbiome from distinct body sites are ecologically unique and altered in insulin resistance

Beyond the influence of personal and environmental factors, we observed distinct ecological attributes among the microbiome at the four body sites (Figure 1E). The stool microbiome exhibited the greatest richness and evenness, underscoring its essential complexity and functional significance. In contrast, the skin microbiome displayed a more skewed population due to its lower evenness compared with the nasal microbiome, despite their similar richness distributions. These ecological features, which often shift with disease progression, aligned with previous findings of IR-related gut dysbiosis,^{25,70} characterized by a significant decrease in stool microbiome's alpha diversity

($t = 2.8462$, $p = 0.0067$). Furthermore, shifts in the richness-evenness scatter plots for all four body sites (Figure S1H) suggested systemic dysbiosis in IR individuals, highlighted by significantly higher skin microbiome richness ($t = -2.9102$, $p = 0.0057$) (Figure S1H) and evenness ($t = -2.4393$, $p = 0.019$) (Figure S1H). These shifts indicate that IR-associated dysbiosis extends beyond the gut microbiome.

Importantly, extending longitudinal observations from single body sites,^{56,94–96} we define a “core microbiome” (see STAR Methods) as microbes consistently present over time, representing potentially indispensable^{97,98} genera at each body sites. Interestingly, we found that stool and oral microbiomes maintain more than 25 highly prevalent core genera, whereas nasal and skin microbiomes only had three (Figure 1F). Importantly, some core genera have low relative abundance, (i.e., *Coprococcus* mean prevalence = 80.75%; mean relative abundance = 0.544%), demonstrating the potential significance of low-abundance strains (Figure S1I). Intriguingly, the richness of core genera in stool and oral microbiome is negatively associated with SSPG (Spearman Rho = -0.52 , $p = 0.00047$) and BMI (Spearman Rho = -0.40 , $p = 0.005$), respectively (Figure S1J), indicating that IR and obesity may be associated with a loss of core microbiomes at these sites.

We further explored the microbiome ecology variations between IR and IS individuals. IR subjects had a significantly higher number of skin core genera ($t = -2.5856$, $p = 0.014$) and a lower number of stool core genera ($t = 2.9659$, $p = 0.0051$) compared with IS individuals (Figure S1K). Notably, several butyrate-producing bacteria (i.e., *Coprococcus*, *Parasutterella*, and *Butyrivibrio*) were decreased in IR stool core microbiomes, whereas diabetes-related opportunistic skin pathogens (i.e., *Finnegoldia*^{99–101} and *Acinetobacter*^{102–105}) were enriched in the skin core microbiome of IR individuals (Table S1C). In addition, we found a clear divergence of the rank prevalence curves in stool and skin microbiome (Figure S1L), demonstrating a global microbial prevalence shift in IR individuals at these two sites.

Additionally, several taxa differed significantly between IR and IS individuals in relative abundance. The stool microbiome of IR individuals showed an increase of genus *Phocaeicola* (Linear discriminant analysis Effect Size [LEfSe]: 0.03; Benjamini-Hochberg [BH] adjusted $p = 0.017$) and a reduction of the genus unclassified *Ruminococcaceae* (LEfSe: 0.017; BH-adjusted $p = 0.0039$), whereas the skin microbiome exhibited a decrease in the genus *Cutibacterium* (LEfSe: 0.069; BH-adjusted $p = 0.007$) and an increase of the genus *Peptoniphilus* (LEfSe: 0.0076; BH-adjusted $p = 0.0022$), which has been previously associated with diabetes-related skin dysbiosis^{100,106,107} and necrotizing infections¹⁰⁸ (Figure S1M; Table S1D). No such differences were observed in oral and nasal microbiomes. These findings further indicate that skin and stool microbiome stability is altered in IR individuals. Overall, our results reveal that IR participants exhibit a stool microbiome with reduced richness and butyrate-producing bacteria, and a skin microbiome more susceptible to opportunistic pathogens.

Distinct taxon-specific stability and individuality in microbiomes across body sites: A potential pathway for personalized interventions

We next examined microbiome stability at the genus level across body sites, hypothesizing stability is taxon and site specific. We

defined a metric “degree of microbial individuality” (DMI, see STAR Methods) for each genus, which quantifies similarity within an individual relative to the population; a high DMI means the microbes taxa is highly individual specific. We also calculated a “family score” (FS, see STAR Methods) to evaluate microbial dissimilarity within households. Expanding observations of the stool microbiome,^{54,70,109} skin, oral, and nasal microbiome also demonstrated significantly less intra-individual and within-family variation compared with the variation observed between different individuals (Figure 2A; Table S2A). Intra-individually, the rate of complete ASV turnover within a genus over time was highest in the nasal microbiome (35.5% of cases), followed by skin (24.4%), stool (24.2%), and oral sites (2.7%). This finding underscores significant intra-individual ecological dynamics at the sub-genus level within microbiomes, despite overall community stability.

The DMI, irrespective of relative abundance, was high in the stool microbiome (Figure 2B), particularly within the *Bacteroidetes* phylum (Figure 2C; Table S2B), possibly due to its pronounced adaptive evolution^{110,111} and substantial colonization resistance.¹¹² Furthermore, the stool microbiome had the lowest FS, whereas oral and nasal microbiomes shared greater similarity within households (Figure S2A), likely due to common living environments^{56,113} or direct microbiome exchanges.¹¹⁴

Our data revealed substantial DMI variance across body sites, potentially attributable to inherent niche-specific taxonomic complexities (Figure 2D; Table S2C). For example, *Corynebacterium* in nasal and *Bacteroides* in stool showed the highest DMI, respectively. These results suggest that specific microbial taxa, adapting to their respective niches, may exhibit enhanced individualization. Therefore, the microbial community at each body site is largely shaped by niche-specific interactions. In contrast, environmental genera such as *Klebsiella*¹¹⁵ and *Haemophilus*¹¹⁶ displayed uniformly low DMI across all examined body sites, indicating that external environmental factors exerts a relatively weaker influence on the individuality of the native host microbiome. Interestingly, after adjusting individuals’ collective DMI by each genera’s relative abundance, we found a notable increase of individuality in the stool microbiomes of IR individuals (Figure S2B), likely due to the increased *Bacteroidetes* among IR individuals.

Overall, the DMI and FS metrics for each specific genus offer an overarching perspective on microbial host specificity. Meanwhile, they provide crucial insights into the taxonomic composition of the community and potential influences of environmental factors on the host’s microbiome. Additionally, the DMI measurements provide important ecological characteristics about micro-biotypes, including “enterotype” in stool microbiome^{78,117} or “cutotypes” in skin microbiome.⁶³

Interplay of microbial individuality and stability: Insights from longitudinal multi-site microbiome analysis

Prior studies^{4,93–95,118–120} demonstrated that microbiome stability is highly personalized. Consequently, we explored the relationship between microbial individuality and stability across body sites. We first examined the genus recolonization rate, measured by ASV consistency when a genus is detectable after being undetected in one or more consecutive samples. The overall recolonization rate (measured by $1 - \text{pairwise}$

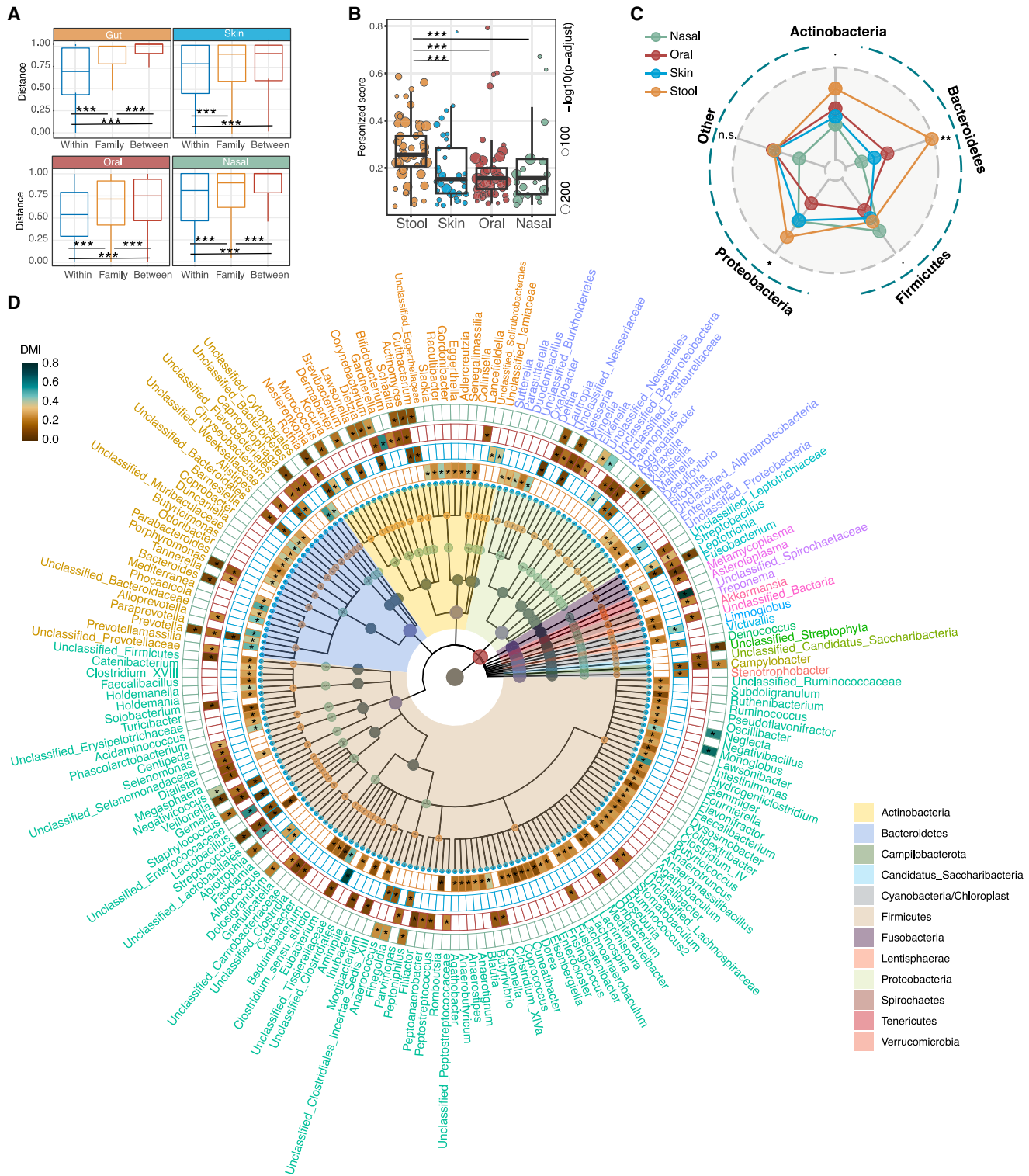


Figure 2. The individuality of the microbiome differs significantly across genera and body sites

(A) Bray-Curtis dissimilarity comparisons within individuals, families, and between unrelated participants.

(B) DMI scores (see STAR Methods).

(C) Average DMI radar plot by body site and phylum, with significant Kruskal-Wallis test results for Actinobacteria, Bacteroidetes, Firmicutes, Proteobacteria, and other phyla.

(D) DMI cladogram representing stool, skin, oral, and nasal microbiomes.

Significance indicated by asterisks: * $p < 0.05$, ** $p < 0.01$, *** $p < 0.001$.

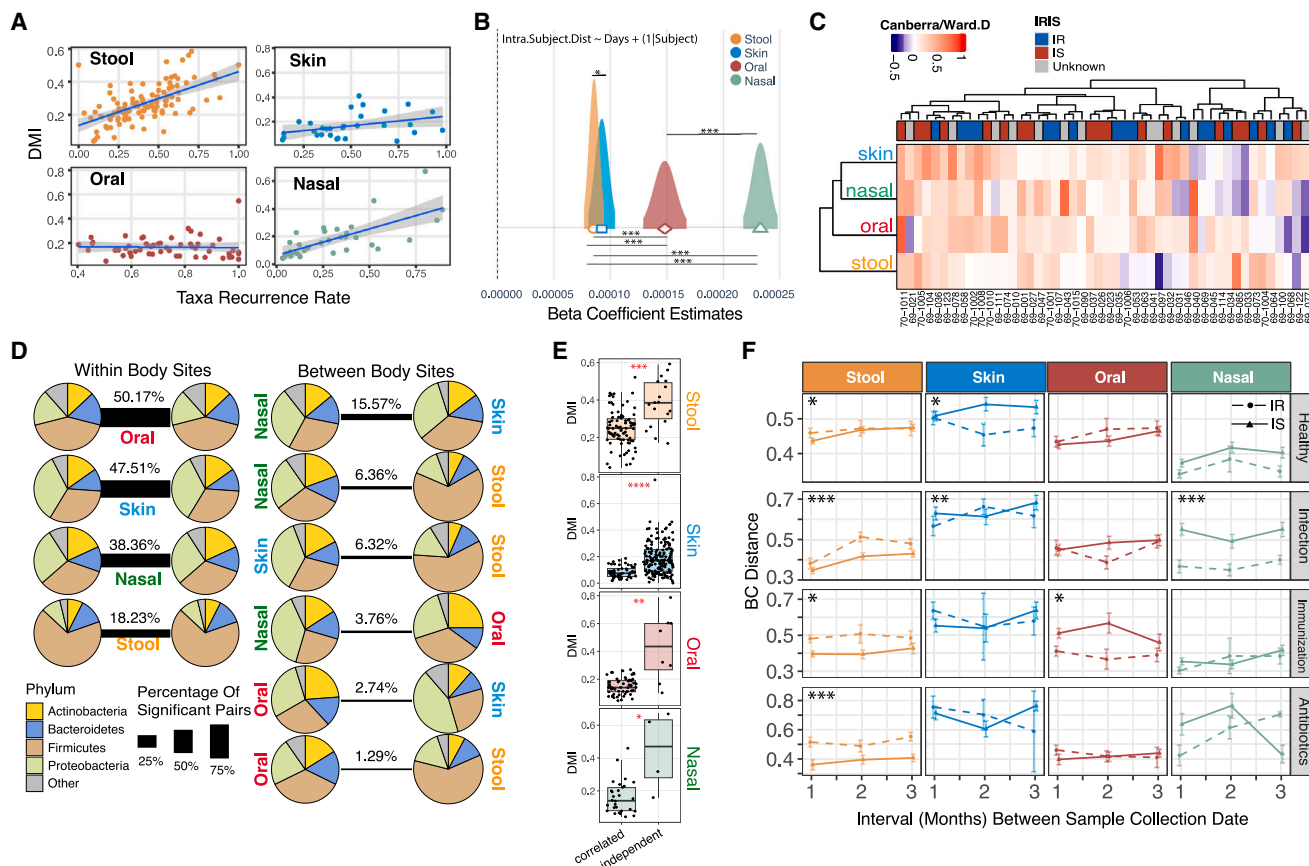


Figure 3. Temporal stability of microbiomes associated with individuality and stress events

(A) Correlations of taxa-recurrence with mean DMI for stool, skin, oral, and nasal samples.
 (B) Linear regression between dissimilarity and collection date interval.
 (C) Beta coefficient of individual-based correlation between sample pair's BC distances and the collection date intervals.
 (D) Correlations of microbiome abundances within and between body sites.
 (E) DMI differences between correlated and non-correlated genera.
 (F) Microbiome shifts during health and stress events over 3 months.
 Significance indicated by asterisks: * $p < 0.05$, ** $p < 0.01$, *** $p < 0.001$.

Jaccard distance^{121,122} was significantly associated with DMI on all three body sites except for the oral microbiome (Figure 3A), which intrinsically maintains a high recolonization rate. Such correlations were strongest in the nasal microbiome (Figure 3A), potentially explaining the high ICC observed above. Surprisingly, no difference in recolonization rate was found between IR and IS individuals (Figure S3A). Our results suggest that highly individualized strains are more likely to recolonize, validating a hypothesis raised by fecal transplantation studies^{123,124} and implying its potential efficacy in treating IR-related dysbiosis.

The longitudinal data also enabled tracking of microbiome stability over time by quantifying the dissimilarity between-sample pairs in relation to collection date intervals, which was reported to be higher in IBD-related gut dysbiosis.¹⁵ Our analysis revealed that the stool microbiome changed more slowly over time, with the nasal site exhibiting the fastest rate of change ($p < 0.001$) (Figure 3B). Additionally, IR individuals showed significantly lower stability in stool and skin microbiomes than IS individuals, as evidenced by linear mixed models (stool $p: 1.82 \times 10^{-6}$, skin $p: 2.84 \times 10^{-12}$), corroborating our findings of greater microbial

abundance disparities in these two body sites between IR and IS participants (Figure S1M).

Intra- and inter-individual correlations of microbiome dynamics across body sites: Implications for microbial interdependence and territory specificity

We next investigated whether microbiome dynamics were intra-individually co-associated across body sites, both at the community level and for individual taxa. Hierarchical clustering demonstrated a strong link in personal microbiome dynamics between the skin and nasal sites, whereas the dynamics of the stool microbiome was less correlated with other body sites (Figure 3C). The inter-site correlation of microbiome stability indicates systemic microbial coordination, potentially regulated by the common mucosal system.^{125,126} Comparison between IS and IR individuals revealed that both groups had a strong skin-nasal link, but a skin-oral correlation was exclusive to IS individuals (Figures S3B and S3C). This implies that IR status undermines the stability of the skin or oral microbiome, possibly due to the compromised host regulation of microbiome stability or

due to impaired mucosal immunity related to IR,¹²⁷ a key factor for between-body-site microbial interactions.^{125,126,128,129}

Since the microbiome often operates as interdependent guilds,^{130–132} we questioned which body sites demonstrate the highest microbial inter-dependency. We found that 18.23% of all stool genus pairings (5,671) were significantly correlated within individuals, mostly *Firmicutes* (Figure 3D). Surprisingly, co-association was highest in the oral microbiome (50.17%), followed by skin (47.51%) and nasal (38.36%), highlighting strong synergistic interactions among microbiome members at each body site (Table S3A).

We further investigated the microbial crosstalk between body sites by searching for sample-wise microbial collinearity. Members from the skin and nasal sites were the most correlated (15.57% of all possible pairs) (Figure 3D; Table S3A). However, remarkable territory specificity was still evident among core microbiomes of each body site (Table S3B). For instance, three predominant core genera—*Corynebacterium*, *Staphylococcus*, and *Cutibacterium*—exhibited no longitudinal correlation between skin and nasal sites. Similarly, oral *Prevotella*'s abundance did not correlate with its abundance in the stool microbiome, consistent with our observation of high FS in oral but not stool *Prevotella* (Table S2C). Although dysbiotic microbiome translocation between body sites has been reported,^{133–135} our results suggest these translocation cases likely do not involve the niche-specific core taxa. Moreover, genera that are more interdependent exhibit lower DMI compared with less interdependent genera (Figures 3E and S3D), indicating that highly individualized microbiomes exhibit greater temporal stability.^{93,136} Expanding on our findings of micro-biotypes across body sites (Figure S1A), we observed that dominant taxa driving these biotypes exhibit significant inter-individual correlations. Examples include significant correlations of *Cutibacterium* levels in one's skin with their *Cutibacterium* level in nasal (beta = 0.56, BH-adjusted $p = 0.0012$), their *Bacteroides* in stool (beta = 0.52, BH-adjusted $p = 0.0038$), and their *Leptotrichia* in oral microbiomes (beta = 0.43, BH-adjusted $p = 0.0088$). Conversely, individuals with high unclassified *Ruminococcaceae* in stool correlates with low *Veillonella* in oral microbiome (beta = -0.35 , BH-adjusted $p = 0.015$) (Table S3C). These findings suggest that the establishment of micro-biotypes are regulated by personalized factors.

Acute events impact microbiome dynamics across body sites and are influenced by insulin resistance

Three strong perturbation events—infection, vaccination, and antibiotic usage—are known to cause stool microbiome disruptions.^{70,76,125,137} Within a 3-month period, the stool microbiome of IR individuals exhibited greater temporal shifts between healthy visits and perturbations than IS individuals (Figure 3F). This pattern, however, was not consistently discernible across other body sites, suggesting a site-specific microbiome response to these events. Unlike IS individuals, IR individuals displayed reduced stool microbiome evenness and lacked the perturbation in nasal microbiome during respiratory infection (Figure S3E), possibly due to higher IR-associated mucosal inflammation^{138–140} masking or superseding infection-induced local microbiome changes observed in IS individuals. During the course of infection, we identified a transient increase in several genera such as *Alistipes* in the stool, *Peptoniphilus* on

the skin, unclassified *Prevotellaceae* in the oral cavity, and *Oribacterium* in the nasal cavity. Conversely, we noticed a decrease in the presence of *Clostridium* cluster IV in the stool, unclassified *Clostridia* in the oral cavity, and unclassified *Neisseriales* in the nasal cavity (Figures S3F–S3H; Table S3D). Although the extent to which transient microbial shifts contribute to IR-related dysbiosis is not clear, the notable increase of core microbiomes in IR skin samples (Figure S1K) may suggest a correlation between acute perturbations and long-term changes in the core microbiome composition. Overall, our findings indicate that dysbiosis can manifest differently across body sites, potentially through site-specific mechanisms. For instance, IR-related temporary disruptions in the stool microbiome seem to be characterized by a loss of core microbiome species producing short chain fatty acids. In contrast, in less complex skin and nasal microbiomes, dysbiosis might involve the acquisition of opportunistic pathogenic species such as *Peptoniphilus*.

The interplay between host immune system and microbiome across body sites: Insights into insulin resistance and inflammation

The dynamics of microbial stability are likely linked to multiple host regulatory mechanisms, particularly the immune system.^{44,129,141–144} Using our customized bayes model,¹⁴⁵ we examined the longitudinal interplay between 62 host circulating cytokines/chemokines, growth factors, and microbiome abundance at all four body sites. Based on credible interval, we identified 477 stool, 226 skin, 318 oral, and 221 nasal significant microbiome-cytokine associations that are body-site specific (Figure 4A; Table S4A). The stool and oral microbiome showed a significantly broader microbiome interaction spectrum than skin and nasal microbiome (Figure 4A). Interestingly, the cytokines associated with epithelial/endothelial growth and vascular inflammation (i.e., epidermal growth factor [EGF], Vascular cell adhesion molecule[VCAM]-1, and interleukin [IL]-22), IL-1 family members (i.e., IL-1b and IL-1Ra), and leptin demonstrated the highest number of interactions with the microbiome. We further identified a subgroup of cytokines including IL-1b, IL-1Ra, MCP3(Chemokine ligand [CCL]-7), and IL-23 as the strongest correlative cytokines with the microbiome via effect size (Figure S4A). The clear pattern of body-site-specific interactions may contribute to the taxa niche specificity. For example, *Moraxella* shows a negative correlation with 23 cytokines on the skin, yet only with three in the nasal cavity (Table S4B). This reduced microbe-immune interaction in the nasal cavity may explain the higher prevalence of *Moraxella* in nasal.^{7,146}

We next examined whether certain phyla are more frequently interacting with cytokines, potentially influencing their stability and individuality. Members of the *Firmicutes* phylum (primarily *Clostridia*) were significantly overrepresented among cytokine-correlated microbes across all body sites ($X_{\text{stool}}^2 = 19.343$, $p_{\text{stool}} = 1.092 \times 10^{-5}$; $X_{\text{skin}}^2 = 10.418$, $p_{\text{skin}} = 0.0012$; $X_{\text{oral}}^2 = 30.935$, $p_{\text{oral}} = 2.668 \times 10^{-8}$; $X_{\text{nasal}}^2 = 31.396$, $p_{\text{nasal}} = 2.104 \times 10^{-8}$) (Figure 4B). This interaction may account for *Firmicutes*' higher FS and lower DMI in the stool microbiome compared with other phyla. Additionally, an increase of *Firmicutes* is associated with conditions like obesity-related gut dysbiosis,¹⁴⁷ IBD-related oral dysbiosis,¹⁴⁸ and psoriasis-related skin dysbiosis,¹⁴⁹ which share inflammation as a common factor.

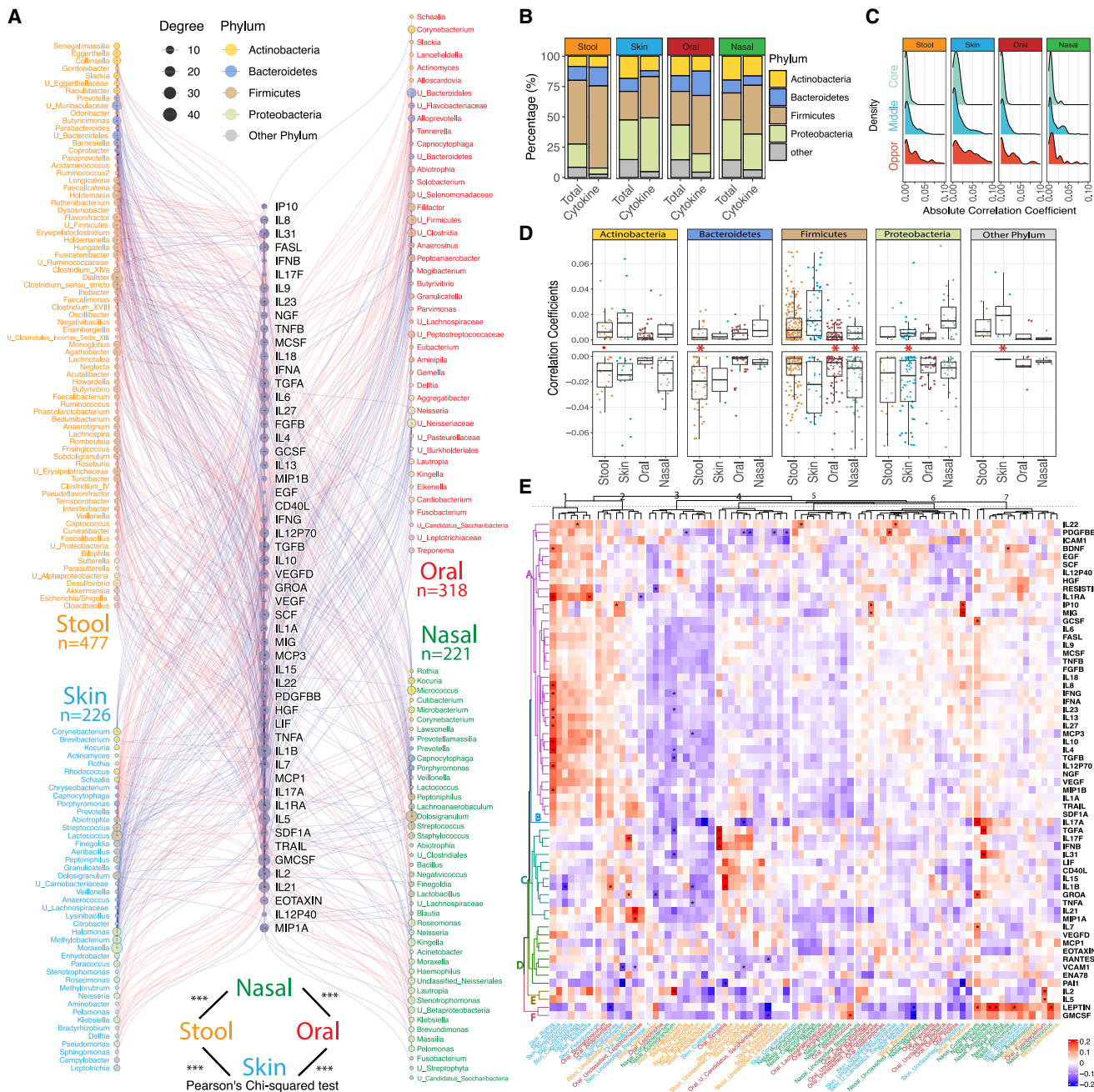


Figure 4. Systematic connections between circulating cytokines and microbiomes

(A) Mixed-effects model outputs for cytokine-microbiome correlations; red lines for positive, blue for negative associations; circle size denotes significant correlation count.

(B) Cytokine-related genera percentages by phylum.

(C) Density plot of significant cytokine-microbiome correlation coefficients compared by genera prevalence.

(D) Correlation coefficients by body site and phylum. p values for positive versus negative associations were annotated in the middle.

(E) Hierarchical clustering of Spearman coefficients between cytokines and diverse genera.

Significance indicated by asterisks: *p < 0.05, **p < 0.01, ***p < 0.001.

Interestingly, cytokines appear to play a pivotal role in shaping an individual's core microbiome and in curbing the colonization of non-commensal bacteria, including many from the *Proteobacteria* phylum. At all four body sites, we found that opportunistic microbes demonstrated a stronger correlation with cytokines

than core microbiomes (see [STAR Methods](#)) (stool: $W = 1,715$, $p = 1.181 \times 10^{-12}$; skin: $W = 223$, $p = 0.004041$; oral: $W = 1,055$, $p = 7.877 \times 10^{-6}$; nasal: $W = 482$, $p = 0.004691$) (Figure 4C). This correlation is largely driven by *Proteobacteria* rather than *Firmicutes*, as *Proteobacteria* consistently constitutes a

larger segment of the opportunistic microbiome compared with the core microbiome (Figure S4B). *Proteobacteria* often carry potent lipopolysaccharides (LPSs) and instigate the downstream immune cascade.^{150–154} Previous studies^{125,155,156} have reported an increase in *Proteobacteria* abundance during inflammation. Contrarily, our study revealed that the correlations between cytokines and *Proteobacteria* abundance are mostly negative, except for *Proteobacteria* members in the nasal microbiome (Figure 4D). The negative correlation of *Proteobacteria* is stronger in stool ($W = 25,315$, $p = 0.04439$), skin ($W = 4,995$, $p = 0.005214$), and oral sites ($W = 9,443$, $p = 9.649 \times 10^{-5}$) but weaker in nasal sites ($W = 5,218$, $p = 0.2693$). Furthermore, all cytokine correlations ($n = 10$) from opportunistic stool *Proteobacteria* are negative, whereas many high-prevalence *Proteobacteria* members exhibit positive correlations with cytokines (Figure S4C). Our results suggest that inflammation might contribute to the adaptation of more prevalent *Proteobacteria*.^{125,157}

The host response by cytokines and chemokines may be linked with the observed richness of bacterial genera, in addition to their relative abundance. We therefore examined the correlation between cytokines and the richness of the 20 most diverse genera per body site. The richness of several prevalent stool microbiome genera within the *Bacteroidetes* phylum, such as *Prevotella*, *Phocaeicola*, and *Parabacteroides*, form a cluster (column 3, Figure 4E) with primarily negative associations, echoing our finding that the relative abundances of *Bacteroidetes* members are more likely to be negatively correlated with cytokines (Figure 4D). Also, leptin and Granulocyte-macrophage colony-stimulating factor (GM-CSF), both strongly associated with BMI (Figure S4D), show the strongest overall correlation with richness (row cluster F, Figure 4E). This extends findings from numerous studies^{147,158–160} on obesity's influence on the gut microbiome diversity to additional body sites. Furthermore, we discovered that seven skin genera (column cluster 1, Figure 4E) positively correlated with a cytokine cluster (row cluster A, Figure 4E), indicating that the richness of specific skin genera (e.g., *Rothia*, *Veillonella*, and *Streptococcus*) is positively associated with the level of plasma cytokines. Consequently, the observed increase in the skin microbiome richness in IR individuals (Figure S6B) may suggest a diminished host selection of the skin microbiome during inflammatory periods.

Overall, our analysis elucidates the interplay between chronic low-grade inflammation and microbial dynamics across various body sites. It connects the immune system with microbiome composition and individualization and sheds lights on how these dynamics are both influenced by and contribute to insulin resistance.

The microbiome is highly connected with host molecules: Unraveling the role in insulin resistance and inflammation

To comprehensively explore the relationship^{67,161,162} between the microbiome and internal host molecules and its role in IR, we analyzed the correlations between microbiome genera and plasma proteins, lipids, and metabolites in the host. We first modularized the lipidomics data to address its high collinearity (Figure S5A; Table S5A) and then applied a linear mixed model to residualize all omics data (see STAR Methods), reducing be-

tween-individual variation and emphasizing longitudinal intra-individual relationships.

Interestingly, the microbiome-host molecule interaction network partitions according to internal molecular composition rather than body sites of the microbiome (Figure 5A), suggesting that certain taxa are primarily influenced by internal molecules interactions over influencing host molecular composition. Notably, three enterotypes driving taxa: *Bacteroides*, *Prevotella*, and unclassified *Ruminococcaceae*, exhibit a clear preference for the lipidome, proteome, and metabolome regions, respectively (Figure 5A; Table S5B). The close association between *Prevotella* and proteins has been previously documented,^{163,164} as well as the relationship between *Bacteroides* and lipids.^{165,166} However, our findings reinforce this understanding to include both additional taxa and multiple body sites, suggesting that these connections are not only site and taxa specific but also systemic and robust.

Many taxa-molecule interactions were consistent across body sites, validating the robustness of these relationships. The skin microbiome exhibited the broadest connectivity in the microbe-lipidome association, whereas the stool microbiome was mainly connected to the metabolome and proteome, as expected^{167,168} (Figure 5B). Proteome pathway annotation further supported these connections and their potential functional implications. The skin microbiome-related proteins were enriched for pathways regulating lipid transport and metabolism, whereas the stool, nasal, and oral microbiomes were more strongly connected to the host immune response, including complement activation and humoral immune response. The oral microbiome exhibited significant associations with proteins linked with regulation of proteolysis, hydrolase activity, and enzyme, peptidase, and lipase inhibitor activity (Figure S5B). Strikingly, the complexity of the network between the stool microbiome and host molecular relationships was significantly reduced in individuals with IR (Figure S5C), indicating a loss of balance in these individuals.

Our study reveals that several metabolites, such as alcohol-associated metabolite ethyl glucuronide,¹⁶⁹ interact with microbiomes across all four body sites, demonstrating a more global effects of alcohol beyond the gut and oral microbiome.^{170–172} Notably, skin *Neisseria* and *Klebsiella*, recognized for their acetaldehyde-^{173,174} and ethanol-producing^{175,176} potential, showed a positive correlation with plasma ethyl glucuronide level (Figure 5C). Conversely, *Faecalimonas*, typically an acetate-producing bacteria^{177,178} and sensitive to alcohol,¹⁷⁹ exhibited a significant negative correlation with ethyl glucuronide. Furthermore, *Desulfovibrio*, a key genus promoting microbiome-related metabolic syndrome,^{180,181} was positively correlated with ethyl glucuronide. These findings suggest that alcohol metabolism is associated with microbial dysbiosis across various body sites.

We also observed notable interactions between microbiome genera richness, a recognized indicator^{182,183} of host metabolic status, and internal plasma analytics. These interactions were most pronounced in the stool microbiome, likely due to its high richness (Figures 5D and S6A; Table S5C). Intriguingly, we discovered a positive association between p-cresol glucuronide, a bacteriostatic¹⁸⁴ metabolite produced exclusively by the anaerobic gut microbiome and linked to insulin resistance,^{27,185} and the richness of unclassified *Ruminococcaceae* and *Oscillibacter* in the stool. Conversely, it was negatively associated with genera typically considered metabolically beneficial, such

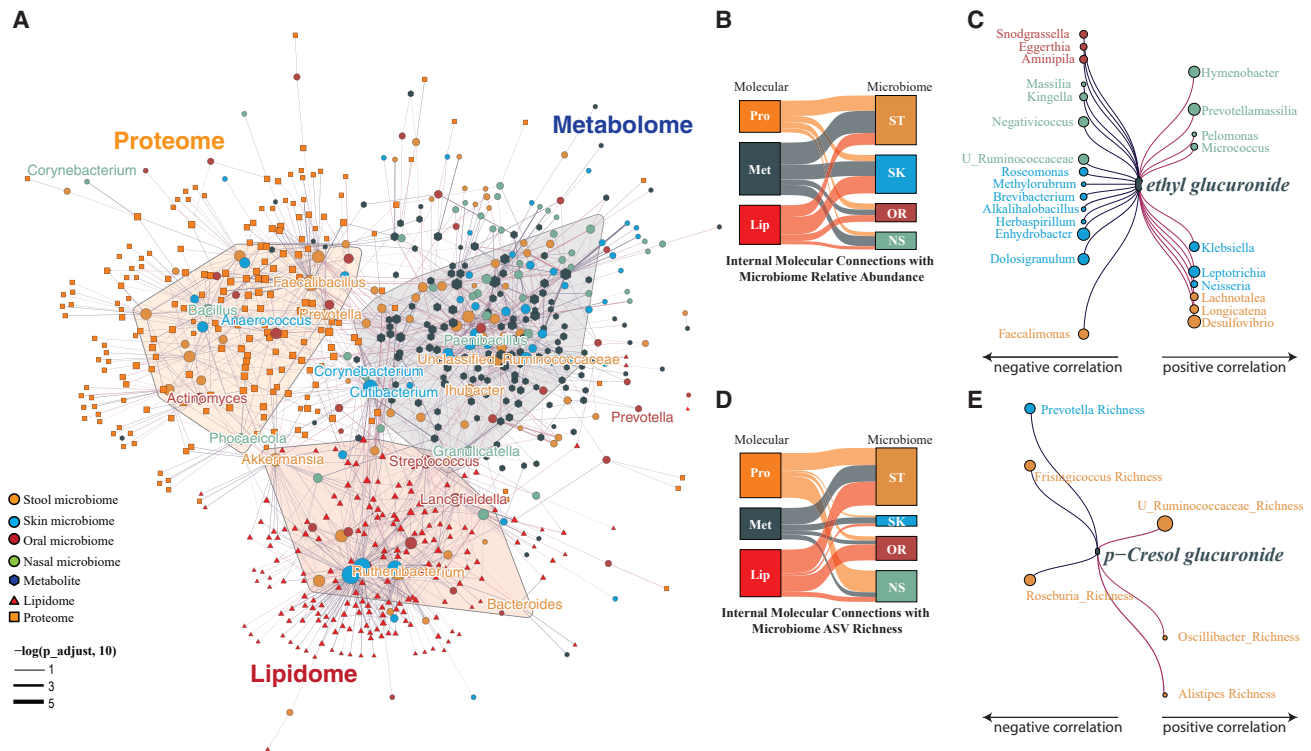


Figure 5. Interactions between plasma metabolites, lipids, proteomics, and microbiome over time

(A) Correlation network shows links between microbiome genera relative abundance and plasma analytics, color-coded by type (microbiomes: dark yellow, blue, dark red, green; plasma analytics: dark blue, orange, red).
 (B) Plasma analytics-microbiome relative abundance correlation summary of (A).
 (C) Correlations between genera and the metabolite ethyl glucuronide.
 (D) Plasma analytics-microbiome relative richness summary of Figure S6A.
 (E) Correlations between genera and the metabolite p-cresol glucuronide.

as *Roseburia*^{186–188} (Figure 5E). These findings suggest that p-cresol glucuronide may influence the development of insulin-resistance-related dysbiosis by altering host tolerance to certain genera belonging to *Clostridia*.

In conclusion, our results not only validate several previous findings but also generate more host-microbial associations, enhancing our understanding of the complex interplay between the human microbiome, metabolites, and host health.

Elucidating microbiome-mediated effects on clinical phenotypes: A comprehensive mediation analysis across four body sites

We next investigated potential causal linkages between microbes, host molecules and clinical phenotypes using mediation analysis.^{189,190} This method measures the contribution of mediators, such as plasma omics or cytokines/chemokines, to the assumed¹⁹¹ microbiome-clinical phenotype (Table S6A) connection, providing confidence levels by inverting the roles of mediator and dependent variable.^{56,189,192} Using this assumption, we identified 330 directionally significant mediation effects involving microbial taxa across all sites, with 207 and 164 of these mediation effects detected in IS and IR participants, respectively (Figure 6A, Table S6B). These outcomes suggest potential microbiome-host causality exists and varies with IR status, though unaccounted confounders remain possible.

Compared with IS, we observed a significant decrease in cytokine-mediated effects of stool microbiome on hematologic parameters ($p = 0.002$) (Figures 6B, 6C) and metabolome-mediated effects of stool microbiome on immune phenotypes ($p = 0.002$) in IR individuals. Furthermore, there was an absence of lipidome-mediated associations between skin microbiome and host plasma lipids/cholesterol in IR participants ($p = 0.031$), suggesting a dysregulation in specific microbiome-metabolic interactions related to hematologic/immune and lipid/cholesterol homeostasis in IR (Figures 6D, 6E, Table S6C). In contrast, the oral microbiome mediated a large proportion of immune profiles via the modulation of lipidome ($p = 0.035$) and cytokines ($p = 0.0001$) in IR relative to IS participants, primarily through a negative relationship among major oral core microbiomes such as *Veillonella* (Table S6B). These causal relationships align with previous findings suggesting that diabetes-related oral dysbiosis may arise from a combination of the loss of core commensal oral taxa^{34,37,193} and an increase in the pathogenicity of resident oral bacteria during impaired glucose metabolism, as demonstrated by human observational studies^{194,195} and animal research.^{36,40}

DISCUSSION

This study presents a systematic analysis of longitudinal multi-site microbiome ecology and host dynamics. With date-matched

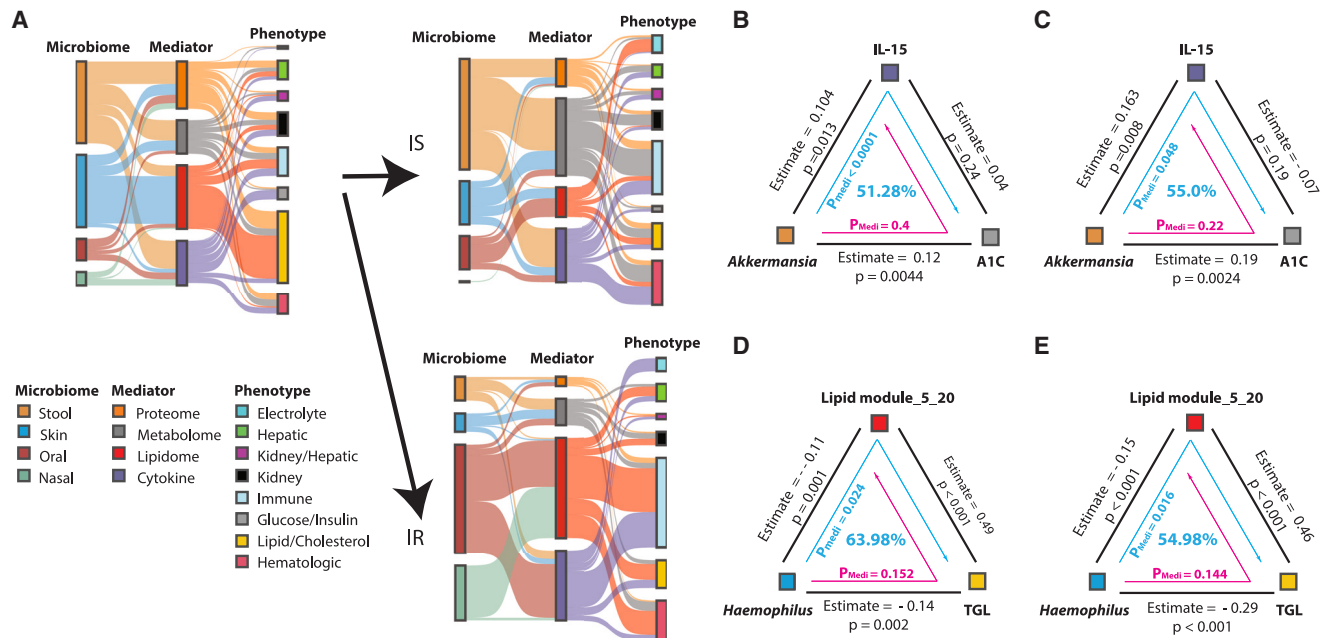


Figure 6. Causal inference decodes microbiome-driven phenotypic dynamics mediated by internal molecules and cytokines
(A) Microbiome and phenotype mediation analysis. Comparisons between IS and IR regarding each mediated effect were performed using a Fisher's exact t test.
(B) *Akkermansia*'s mediation effect on blood A1C level via plasma IL-15.
(C) *Akkermansia*'s mediation effect on blood A1C level in insulin sensitive individuals.
(D) *Haemophilus*'s mediation effect on plasma triglycerides level.
(E) *Haemophilus*'s mediation effect on plasma triglycerides level in insulin sensitive individuals.

microbiome and host omics, we not only expand our knowledge of the stability and individuality of microbiome from various body sites but also provide mechanism-generating hypotheses on host-microbiome interactions in the context of prediabetes. We demonstrate a number of interesting observations: (1) there is a "core" microbiome that is highly stable over time and an opportunistic microbiome that is highly variable and more potent to the immune system; these are niche specific. (2) Correlations between microbiomes across body sites and extensive interactions with host factors indicate systemic coordination and interactions across the human body. (3) Highly individualized microbiomes are associated with distinct environmental factors (i.e., season, diet, chemical, and biological exposome) in a niche-specific manner. However, these effects do not override the variance contributed by individuals, suggesting that the host is still the largest confounding factor for the variation observed in the microbiome. (4) Individuals with IR have a less stable microbiome with more diverse microbiome members on skin, possibly associated with upper respiratory infection, as well as significantly altered host-microbiome interactions.

Our study revealed that the stool and oral microbiomes exhibit the highest level of individualization, likely due to the unique influence of personalized dietary habits and host-specific factors, such as IR, impacting the digestive system.¹⁹⁶ Meanwhile, the skin and nasal microbiomes are less individualized, possibly owing more to individual environmental exposure.^{90,113} We observed site-specific impact of environmental factors, such as season, on the microbiomes of these four body sites. For instance, a decrease in stool microbiome rich-

ness in late summer corresponded with previous findings of worsened insulin sensitivity during this period.^{197,198} Similarly, we noted a decline in the richness and evenness of the oral microbiome from late summer through winter, suggesting a potential influence of environmental factors like the availability of fresh food and changes in sunlight durations. Meanwhile, changes in humidity from January to April might explain the richness increase in skin and decrease in nasal microbiome.⁹⁰ These observations underscore the critical role of the host in modulating the microbiome in response to environmental fluctuations.

Leveraging dense longitudinal sampling, we were able to quantify the stability and degree of individuality of the microbiomes at different body sites. The strong correlation between microbiome stability and individuality suggests an active role of the host in the establishment of commensal bacterial populations. Notably, this individuality appears to be taxon specific, pointing to the possibility that the stability of an individual's microbiome may be influenced by the dominant bacterial taxa they carry. For instance, the higher DMI in stool *Bacteroidetes* links traditional *Bacteroidetes/Firmicutes* ratio or enterotypes to new insights in the context of metabolic disorders.^{117,199} Furthermore, micro-biotypes across different body sites within the same individual correlate. Individuals with high levels of *Bacteroides* in the stool also have high *Cutibacterium* on the skin and *Prevotella* in the oral microbiome. Combined with our findings on the correlation between microbiome individuality and stability, the low-level engagement between the core microbiome and cytokines, and the clear host molecular

type-specific patterns in the host-microbiome interactome, we propose that the colonization and adaptation of bacteria across multiple body sites is not random but precisely regulated by host factors.

Niche-specific traits often emerge through multi-site comparisons; for instance, we identified unique characteristics of the oral microbiome. The recurrence rate of oral bacteria does not increase with DMI, possibly due to a stable and conserved community structure within the oral microbiome.^{83,200} This, coupled with the oral microbiome's high intra-site interdependence and minimal correlation with other body sites, underscores its specialization. The unique oral environment, shaped by factors such as saliva, teeth, gums, tongue, and distinct nutrient availability, likely contributes to this specialization.^{201,202}

Microbial individuality and stability are closely related to the host immune system, which is well known to interact with microbes at multiple body sites.^{141,203,204} This interaction modulates both the colonization of microbes, as well as their functional benefits (e.g., epithelium barrier integrity maintainance^{44,205}). Our Bayesian model reveals that the interactions between the microbiome and cytokines, while present, are subtle. Certain genera exhibit an approximate 1.5-fold change in response to cytokine variations. The interaction between inflammatory cytokines and the microbiome demonstrated that low prevalence genera (i.e., stool *Proteobacteria*) are likely reduced during host inflammatory events. We also revealed a systematic relationship between cytokines and the genera complexity of the microbiome at each body site. Notably, the diversity within a subset of the skin microbiome positively correlates, while that within the stool microbiome negatively correlates with the same group of cytokines. Given the established association of IR with low-grade chronic inflammation,²⁰⁶ the observed changes in diversity among IR individuals might be related to their unique cytokine profiles.

We also identified a list of interactions between host plasma biomolecules and microbiomes (Table S5B). Some of the relationships, such as alcohol metabolites and the gut microbiome, have been documented.^{207,208} We also find many correlations across body sites with host factors; for example, the correlated *Bacteroides* in the stool and *Cutibacterium* in the skin are both closely related to lipid metabolism.^{209–213} Our multi-omics analyses suggest potential causality of host factors in these relationships, reinforcing the idea of host-driven systematic microbial coordination across body sites as proposed in gut-brain axis^{214,215} and gut-lung axis^{216,217} theories. Since many of the metabolites, lipids and proteins are signaling molecules (e.g., chemokines, hormones, and peptides), these molecules may play important roles in organismal communication across the entire host-microbiome ecosystem. Importantly, this interaction presumably occurs individually, and significantly altered at disease stage.

Intriguingly, we found *Klebsiella* on skin was positively associated with metabolites of alcohol. This indicates that alcohol intake may change the host into a *Klebsiella*-tolerant environment, resulting in the adaptation and expansion of pathogenic *Klebsiella* as previously described.²¹⁸ This observation supports previous findings in alcohol-associated pneumonia, where alcohol consumption and increased susceptibility to *Klebsiella* in the lungs may be a result of either intestinal *Klebsiella*-specific T cell sequestration^{218,219} or alcohol-related

impairment of tryptophan catabolite production/processing in the gut microbiome, which restricts pulmonary immune cell trafficking.^{220,221}

Insulin resistance (IR) appears to disrupt the intricate balance between the host and microbiome, demonstrated by an unstable, dysbiotic microbiome in IR individuals. In our study, we discovered marked differences in the microbiome composition, diversity, and core members of the stool and skin microbiomes in IR individuals compared with their IS counterparts. Notably, the systematic shift in microbiome prevalence indicates an entire microbial community's transformation instead of the abnormality of a few isolated members (Figure S1L). This dysbiosis can potentially alter the complex host-microbiome interaction in IR subjects. Consistently, we detected reduced host-microbe coordination and a missing association between oral and skin microbiome stability. Further, our mediation analysis validates our result about the reduced gut microbiome-cytokine interaction in IR individuals^{70,145} and reveals heightened pro-inflammatory signals linked to the microbiomes of the upper respiratory tract (oral and nasal microbiome) in IR individuals. Our in-depth exploration of acute microbiome changes during infection provides additional substantiation for this theory. We observed a significant increase in IR-enriched skin genera such as *Peptoniphilus* and *Intrasporangium* (Figure S3D) during the course of a respiratory viral infection, while a decline in specific genera in the stool microbiome known for butyrate production, like *Clostridium_IV*, *Lawsonibacter*, and *Intestinimonas*.^{222–225} While these findings do not explicitly validate the hypothetical link²²⁶ between respiratory viral infection, chronic metabolic dysregulation, and related complications, they suggest that infection-related microbial shifts may be associated with, or even cause, the dysbiosis and complications of metabolic syndrome as observed in animal models.²²⁷

Limitations of the study

Caution is warranted in interpreting our results due to inherent limitations. The DMI and FS calculations primarily rely on the Bray-Curtis (BC) dissimilarity. Therefore, study design such as sample size, population representation, choice of dissimilarity metric, and genus internal complexity may impact the accuracy. Additionally, although DMI can provide a quantitative measure of microbiome individuality, understanding its biological or ecological significance can be challenging due to the potential influence of host genetics, environmental factors, and host regulation.

When the study began, 16S rRNA sequencing was highly efficient for analyzing microbiomes rich in human DNA, such as those in nasal and skin swabs. However, our team, along with others, later identified its limitations in accurately capturing specific bacterial genera in stool and skin microbiomes when focusing on only certain variable regions.^{73,228} Furthermore, unlike metagenomic sequencing, 16S analysis does not provide information on viruses and fungi within a microbiome community, nor does it reveal gene function potentials. Also, our study does not capture a collective profile of the entire skin or oral microbiome, given the distinct characteristics of species at various sites.^{7,62,119} Instead, it represents the microbiome from a single swab taken from each indicated body site. Furthermore, the geographical and lifestyle constraints of our participants could restrict the broad applicability of our conclusions to more diverse and complex populations.^{229,230} Moreover, we note that our

analyses primarily determine associations or statistical mediation effects, using p values as cutoffs. Despite the bolstered study power afforded by a longitudinal design,^{231,232} some observations with a smaller sample or effect size may still be overlooked. Analysis of larger cohorts may reveal further insights. Additionally, the use of p values has its limitations regardless of the cutoff,²³³ such as its dependence on sample size,²³⁴ the potential for misinterpretation,^{235,236} and an inflated type 1 error rate with multiple tests.^{237,238} Finally, while our study highlights notable associations and suggests potential causations, it does not establish causation. Our mediation analysis aims to infer directionality and potential causality, but unobserved factors could influence these findings. To confirm causative links, more targeted follow-up studies are essential.

In spite of these limitations, our studies provide a number of observations concerning the individuality and stability of the microbiome across multiple body sites during health and disease and in individuals with different IR/IS status. These observations have important implications in modulation human molecular health using personalized prebiotics and probiotics. Our data also provide a valuable and unique resource for the general scientific community.

STAR★METHODS

Detailed methods are provided in the online version of this paper and include the following:

- **KEY RESOURCES TABLE**
- **RESOURCE AVAILABILITY**
 - Lead contact
 - Materials availability
 - Data and code availability
- **EXPERIMENTAL MODEL AND SUBJECT DETAILS**
 - Human Cohort
- **METHOD DETAILS**
 - Microbiome sample collection and sequencing
 - Microbiome data processing
 - Lipidomics analyses
 - Metabolomics Analyses
 - Proteomics analyses
 - Luminex multiplex assays for targeted cytokine, chemokine, and growth factors
 - Exposome and associated environmental analyses
 - Dietary analyses
 - Insulin-suppression test
 - Clinical lab test
- **QUANTIFICATION AND STATISTICAL ANALYSIS**
 - UMAP for microbiome distribution
 - Intra-class correlation
 - Permutation test on Bray-Curtis Distance Comparison
 - Degree of microbial individuality
 - Family score
 - Classification of the microbiome genera by their longitudinal prevalence
 - Body site-specific longitudinal model for Bray-Curtis distance
 - Bayesian mixed-effects model for microbial taxa and cytokine interactions

- Correlation network analysis
- Pathway enrichment for proteins correlated with the microbiome
- Mediation analysis
- Principal variance component analysis (PVCA)
- Deconvolute the environmental effect on the microbiome

SUPPLEMENTAL INFORMATION

Supplemental information can be found online at <https://doi.org/10.1016/j.chom.2024.02.012>.

ACKNOWLEDGMENTS

We extend our sincere gratitude to all research participants for their dedication and involvement. We are grateful for the valuable insights provided by the members of Snyder Lab (Stanford University) and Weinstock Lab (The Jackson Laboratory of Genomic Medicine). Our thanks also go to Mrs. Ada Yee Ki Chen and Mrs. Lisa Stainton for their research administrative support. Our appreciation extends to the Stanford Immune Monitoring Core and Ms. Yael Rosenberg-Hasson for their contribution to the cytokine Luminex Multiplex Assay. We also thank Dr. Victor Felix and Dr. Owen White (University of Maryland) for their assistance in uploading our raw sequencing data to the iHMP portal. We thank artist Lettie McGuire EdM for her help with the graphical abstract and cover design. This work was funded by National Institutes of Health (NIH) Common Fund Human Microbiome Project U54_DE0237891, NIH U54_DK102556, NIH R01_DK110186, NIH S10_OD020141, NIH R01 AT010232-04, NIH UL1 TR001085, NIH P30_DK116074, S10_OD023452. We are also sincerely grateful for the generous support from Leona M. and Harry B. Helmsley Charitable Trust (grant no. G-2004-03820), the Innovative Medicines Accelerator (grant no. IMA-1051) grant, and the RAMBAM-Stanford International Collaboration grant at Stanford University. We acknowledge the fellowship support received by X. Zhou from the Stanford Aging and Ethnogeriatrics (SAGE) Research Center under NIH/NIA Resource Centers for Minority Aging Research grant P30AG059307, S.M.S.-F.R. from the NIH K08 ES028825, A.W.B. from 1F32DK126287, D.J.S. from NIA-K01AG070310, and J.S.J. from the Kennedy Trust for Rheumatology Research. Some of the icons in the summary figure were created with [Biorender.com](https://biorender.com).

AUTHOR CONTRIBUTIONS

X. Zhou, X.S., J.S.J., D.J.S., G.M.W., and M.P.S. conceptualized the study and devised the analysis plan. X. Zhou, W.Z., M. Agnello, S.L., and M. Avina oversaw the comprehensive sample collection and conducted experimental benchmark. X. Zhou, W.Z., S.L., Y.Z., L.C., L.L., and E.J.B. were responsible for microbiome data acquisition and processing. D.H. and S.W. handled lipidome data acquisition and processing. C.J., Liuyiqi Jiang, X. Zhang, and X.S. undertook exposome data acquisition and processing. X. Zhou, W.Z., and P.K. executed cytokine Luminex assay data acquisition and analysis. Lihua Jiang and R.J. performed proteome data acquisition and analysis. K. Contrepolis and X.S. managed metabolomics data acquisition and analysis. J.S.J., D.J.S., X. Zhou, and X.S. designed and implemented longitudinal data modeling. W.Z., M. Avina, S.L., A.C., and A.W.B. coordinated participants' clinical visits and sample collection/inventory. X. Zhou, X.S., J.S.J., and C.Z. carried out integrative omics analysis. X. Zhou and X.S. conducted the bootstrap and permutation analysis. M.P.S. and G.M.W. provided funding support and overall project supervision. X. Zhou, A.H., and S.J.C. provided additional data visualization. X. Zhou completed the data and code organization and publication. X. Zhou, J.S.J., D.J.S., and M.P.S. wrote the manuscript with contributions from all listed authors.

DECLARATION OF INTERESTS

M.P.S. is a co-founder and the scientific advisory board member of Personalis, Qbio, January, SensOmics, Filtricine, Akna, Protos, Mirvie, NiMo, Onza, Oralome, Marble Therapeutics, and Iollo. He is also on the scientific advisory

board of Danaher, Genapsys, and Jupiter. A.H. is a founder and shareholder of Arxeon. Y.Z. and G.M.W. are co-founders of General Biomics.

DECLARATION OF GENERATIVE AI AND AI-ASSISTED TECHNOLOGIES IN THE WRITING PROCESS

During the preparation of this work the author(s) used ChatGPT in order to improve the quality of scientific writing. After using this tool/service, the author(s) reviewed and edited the content as needed and take(s) full responsibility for the content of the publication.

Received: December 5, 2023

Revised: January 23, 2024

Accepted: February 20, 2024

Published: March 12, 2024

REFERENCES

1. Qin, J., Li, R., Raes, J., Arumugam, M., Burgdorf, K.S., Manichanh, C., Nielsen, T., Pons, N., Levenez, F., Yamada, T., et al. (2010). A human gut microbial gene catalogue established by metagenomic sequencing. *Nature* 464, 59–65.
2. Gilbert, J.A., Blaser, M.J., Caporaso, J.G., Jansson, J.K., Lynch, S.V., and Knight, R. (2018). Current understanding of the human microbiome. *Nat. Med.* 24, 392–400.
3. Ursell, L.K., Metcalf, J.L., Parfrey, L.W., and Knight, R. (2012). Defining the human microbiome. *Nutr. Rev.* 70, S38–S44.
4. Oh, J., Byrd, A.L., Park, M., NISC Comparative Sequencing Program, Kong, H.H., and Segre, J.A. (2016). Temporal Stability of the Human Skin Microbiome. *Cell* 165, 854–866.
5. Roswall, J., Olsson, L.M., Kovatcheva-Datchary, P., Nilsson, S., Tremaroli, V., Simon, M.C., Klierich, P., Akrami, R., Krämer, M., Uhlén, M., et al. (2021). Developmental trajectory of the healthy human gut microbiota during the first 5 years of life. *Cell Host Microbe* 29, 765–776.e3.
6. Zhou, Y., Gao, H., Mihindukulasuriya, K.A., La Rosa, P.S., Wylie, K.M., Vishnivetskaya, T., Podar, M., Warner, B., Tarr, P.I., Nelson, D.E., et al. (2013). Biogeography of the ecosystems of the healthy human body. *Genome Biol.* 14, R1.
7. Human Microbiome Project Consortium (2012). Structure, function and diversity of the healthy human microbiome. *Nature* 486, 207–214.
8. Zhou, Y., Mihindukulasuriya, K.A., Gao, H., La Rosa, P.S., Wylie, K.M., Martin, J.C., Kota, K., Shannon, W.D., Mitreva, M., Sodergren, E., and Weinstock, G.M. (2014). Exploration of bacterial community classes in major human habitats. *Genome Biol.* 15, R66.
9. DiGiulio, D.B., Callahan, B.J., McMurdie, P.J., Costello, E.K., Lyell, D.J., Robaczewska, A., Sun, C.L., Goltsman, D.S., Wong, R.J., Shaw, G., et al. (2015). Temporal and spatial variation of the human microbiota during pregnancy. *Proc. Natl. Acad. Sci. USA* 112, 11060–11065.
10. Zhernakova, A., Kurilshikov, A., Bonder, M.J., Tigchelaar, E.F., Schirmer, M., Vatanen, T., Mujagic, Z., Vila, A.V., Falony, G., Vieira-Silva, S., et al. (2016). Population-based metagenomics analysis reveals markers for gut microbiome composition and diversity. *Science* 352, 565–569.
11. Wilmanski, T., Diener, C., Rappaport, N., Patwardhan, S., Wiedrick, J., Lapidus, J., Earls, J.C., Zimmer, A., Glusman, G., Robinson, M., et al. (2021). Gut microbiome pattern reflects healthy ageing and predicts survival in humans. *Nat. Metab.* 3, 274–286.
12. Bana, B., and Cabreiro, F. (2019). The Microbiome and Aging. *Annu. Rev. Genet.* 53, 239–261.
13. Zhou, X., Wang, B., Demkowicz, P.C., Johnson, J.S., Chen, Y., Spakowicz, D.J., Zhou, Y., Dorsett, Y., Chen, L., Sodergren, E., et al. (2022). Exploratory studies of oral and fecal microbiome in healthy human aging. *Front. Aging* 3, 1002405.
14. Zhang, Y., Bhosle, A., Bae, S., Mclver, L.J., Pishchany, G., Accorsi, E.K., Thompson, K.N., Arze, C., Wang, Y., Subramanian, A., et al. (2022). Discovery of bioactive microbial gene products in inflammatory bowel disease. *Nature* 606, 754–760.
15. Lloyd-Price, J., Arze, C., Ananthkrishnan, A.N., Schirmer, M., Avila-Pacheco, J., Poon, T.W., Andrews, E., Ajami, N.J., Bonham, K.S., Brislawn, C.J., et al. (2019). Multi-omics of the gut microbial ecosystem in inflammatory bowel diseases. *Nature* 569, 655–662.
16. Fornelos, N., Franzosa, E.A., Bishai, J., Annand, J.W., Oka, A., Lloyd-Price, J., Arthur, T.D., Garner, A., Avila-Pacheco, J., Haiser, H.J., et al. (2020). Growth effects of N-acyl ethanolamines on gut bacteria reflect altered bacterial abundances in inflammatory bowel disease. *Nat. Microbiol.* 5, 486–497.
17. Nemet, I., Saha, P.P., Gupta, N., Zhu, W., Romano, K.A., Skye, S.M., Cajka, T., Mohan, M.L., Li, L., Wu, Y., et al. (2020). A Cardiovascular Disease-Linked Gut Microbial Metabolite Acts via Adrenergic Receptors. *Cell* 180, 862–877.e22.
18. Walker, R.L., Vlamakis, H., Lee, J.W.J., Besse, L.A., Xanthakis, V., Vasani, R.S., Shaw, S.Y., and Xavier, R.J. (2021). Population study of the gut microbiome: associations with diet, lifestyle, and cardiometabolic disease. *Genome Med.* 13, 188.
19. Fromentin, S., Forslund, S.K., Chechi, K., Aron-Wisnewsky, J., Chakaroun, R., Nielsen, T., Tremaroli, V., Ji, B., Prifti, E., Myridakis, A., et al. (2022). Microbiome and metabolome features of the cardiometabolic disease spectrum. *Nat. Med.* 28, 303–314.
20. Qi, Q., Li, J., Yu, B., Moon, J.Y., Chai, J.C., Merino, J., Hu, J., Ruiz-Canela, M., Rebholz, C., Wang, Z., et al. (2022). Host and gut microbial tryptophan metabolism and type 2 diabetes: an integrative analysis of host genetics, diet, gut microbiome and circulating metabolites in cohort studies. *Gut* 71, 1095–1105.
21. Wu, H., Tremaroli, V., Schmidt, C., Lundqvist, A., Olsson, L.M., Krämer, M., Gummesson, A., Perkins, R., Bergström, G., and Bäckhed, F. (2020). The Gut Microbiota in Prediabetes and Diabetes: A Population-Based Cross-Sectional Study. *Cell Metab.* 32, 379–390.e3.
22. Forslund, K., Hildebrand, F., Nielsen, T., Falony, G., Le Chatelier, E., Sunagawa, S., Prifti, E., Vieira-Silva, S., Gudmundsdottir, V., Pedersen, H.K., et al. (2017). Corrigendum: Disentangling type 2 diabetes and metformin treatment signatures in the human gut microbiota. *Nature* 545, 116.
23. Pedersen, H.K., Gudmundsdottir, V., Nielsen, H.B., Hyötyläinen, T., Nielsen, T., Jensen, B.A., Forslund, K., Hildebrand, F., Prifti, E., Falony, G., et al. (2016). Human gut microbes impact host serum metabolome and insulin sensitivity. *Nature* 535, 376–381.
24. Ruuskanen, M.O., Erawijantari, P.P., Havulinna, A.S., Liu, Y., Méric, G., Tuomilehto, J., Inouye, M., Jousilahti, P., Salomaa, V., Jain, M., et al. (2022). Gut Microbiome Composition Is Predictive of Incident Type 2 Diabetes in a Population Cohort of 5,572 Finnish Adults. *Diabetes Care* 45, 811–818.
25. Chen, Z., Radjabzadeh, D., Chen, L., Kurilshikov, A., Kavousi, M., Ahmadizar, F., Ikram, M.A., Uitterlinden, A.G., Zhernakova, A., Fu, J., et al. (2021). Association of Insulin Resistance and Type 2 Diabetes With Gut Microbial Diversity: A Microbiome-Wide Analysis From Population Studies. *JAMA Netw. Open* 4, e2118811.
26. Deng, K., Shuai, M., Zhang, Z., Jiang, Z., Fu, Y., Shen, L., Zheng, J.S., and Chen, Y.M. (2022). Temporal relationship among adiposity, gut microbiota, and insulin resistance in a longitudinal human cohort. *BMC Med.* 20, 171.
27. Khan, M.T., Nieuwdorp, M., and Bäckhed, F. (2014). Microbial modulation of insulin sensitivity. *Cell Metab.* 20, 753–760.
28. Forslund, K., Hildebrand, F., Nielsen, T., Falony, G., Le Chatelier, E., Sunagawa, S., Prifti, E., Vieira-Silva, S., Gudmundsdottir, V., Pedersen, H.K., et al. (2015). Disentangling type 2 diabetes and metformin treatment signatures in the human gut microbiota. *Nature* 528, 262–266.
29. Al-Muhanna, F.A., Dowdell, A.K., Al Elegg, A.H., Albaker, W.I., Brooks, A.W., Al-Sultan, A.I., Al-Rubaish, A.M., Alkharshah, K.R., Sulaiman, R.M., Al-Quorain, A.A., et al. (2022). Gut microbiota analyses of Saudi

- populations for type 2 diabetes-related phenotypes reveals significant association. *BMC Microbiol.* 22, 301.
30. Gardiner, M., Vicaretti, M., Sparks, J., Bansal, S., Bush, S., Liu, M., Darling, A., Harry, E., and Burke, C.M. (2017). A longitudinal study of the diabetic skin and wound microbiome. *PeerJ* 5, e3543.
 31. Redel, H., Gao, Z., Li, H., Alekseyenko, A.V., Zhou, Y., Perez-Perez, G.I., Weinstock, G., Sodergren, E., and Blaser, M.J. (2013). Quantitation and composition of cutaneous microbiota in diabetic and nondiabetic men. *J. Infect. Dis.* 207, 1105–1114.
 32. Tai, J., Han, M.S., Kwak, J., and Kim, T.H. (2021). Association Between Microbiota and Nasal Mucosal Diseases in terms of Immunity. *Int. J. Mol. Sci.* 22, 4744.
 33. De Pessemer, B., Grine, L., Debaere, M., Maes, A., Paetzold, B., and Callewaert, C. (2021). Gut-Skin Axis: Current Knowledge of the Interrelationship between Microbial Dysbiosis and Skin Conditions. *Microorganisms* 9, 353.
 34. Besnard, P., Christensen, J.E., Bernard, A., Simoneau-Robin, I., Collet, X., Verges, B., and Burcelin, R. (2020). Identification of an oral microbiota signature associated with an impaired olfactory perception of lipids in insulin-resistant patients. *Acta Diabetol.* 57, 1445–1451.
 35. Demmer, R.T., Trinh, P., Rosenbaum, M., Li, G., LeDuc, C., Leibel, R., González, A., Knight, R., Paster, B., Colombo, P.C., et al. (2019). Subgingival Microbiota and Longitudinal Glucose Change: The Oral Infections, Glucose Intolerance and Insulin Resistance Study (ORIGINS). *J. Dent. Res.* 98, 1488–1496.
 36. Xiao, E., Mattos, M., Vieira, G.H.A., Chen, S., Corrêa, J.D., Wu, Y., Albiero, M.L., Bittinger, K., and Graves, D.T. (2017). Diabetes Enhances IL-17 Expression and Alters the Oral Microbiome to Increase Its Pathogenicity. *Cell Host Microbe* 22, 120–128.e4.
 37. Almeida-Santos, A., Martins-Mendes, D., Gayà-Vidal, M., Pérez-Pardal, L., and Beja-Pereira, A. (2021). Characterization of the Oral Microbiome of Medicated Type-2 Diabetes Patients. *Front. Microbiol.* 12, 610370.
 38. Negrini, T.C., Carlos, I.Z., Duque, C., Caiaffa, K.S., and Arthur, R.A. (2021). Interplay Among the Oral Microbiome, Oral Cavity Conditions, the Host Immune Response, Diabetes Mellitus, and Its Associated-Risk Factors—An Overview. *Front. Oral Health* 2, 697428.
 39. Demmer, R.T., Jacobs, D.R., Jr., Singh, R., Zuk, A., Rosenbaum, M., Papapanou, P.N., and Desvarieux, M. (2015). Periodontal Bacteria and Prediabetes Prevalence in ORIGINS: The Oral Infections, Glucose Intolerance, and Insulin Resistance Study. *J. Dent. Res.* 94 (Supplement), 201S–211S.
 40. Watanabe, K., Katagiri, S., Takahashi, H., Sasaki, N., Maekawa, S., Komazaki, R., Hatasa, M., Kitajima, Y., Maruyama, Y., Shiba, T., et al. (2021). *Porphyromonas gingivalis* impairs glucose uptake in skeletal muscle associated with altering gut microbiota. *FASEB J.* 35, e21171.
 41. Vrieze, A., Van Nood, E., Holleman, F., Salojarvi, J., Kootte, R.S., Bartelsman, J.F., Dallinga-Thie, G.M., Ackermans, M.T., Serlie, M.J., Oozeer, R., et al. (2012). Transfer of intestinal microbiota from lean donors increases insulin sensitivity in individuals with metabolic syndrome. *Gastroenterology* 143, 913–6.e7.
 42. Giongo, A., Gano, K.A., Crabb, D.B., Mukherjee, N., Novelo, L.L., Casella, G., Drew, J.C., Ilonen, J., Knip, M., Hyöty, H., et al. (2011). Toward defining the autoimmune microbiome for type 1 diabetes. *ISME J.* 5, 82–91.
 43. Frost, F., Kacprowski, T., Rühlemann, M., Pietzner, M., Bang, C., Franke, A., Nauck, M., Völker, U., Völzke, H., Dörr, M., et al. (2021). Long-term instability of the intestinal microbiome is associated with metabolic liver disease, low microbiota diversity, diabetes mellitus and impaired exocrine pancreatic function. *Gut* 70, 522–530.
 44. Kawano, Y., Edwards, M., Huang, Y., Bilate, A.M., Araujo, L.P., Tanoue, T., Atarashi, K., Ladinsky, M.S., Reiner, S.L., Wang, H.H., et al. (2022). Microbiota imbalance induced by dietary sugar disrupts immune-mediated protection from metabolic syndrome. *Cell* 185, 3501–3519.e20.
 45. Massier, L., Chakaroun, R., Tabei, S., Crane, A., Didt, K.D., Fallmann, J., von Bergen, M., Haange, S.B., Heyne, H., Stumvoll, M., et al. (2020). Adipose tissue derived bacteria are associated with inflammation in obesity and type 2 diabetes. *Gut* 69, 1796–1806.
 46. Amar, J., Chabo, C., Waget, A., Klopp, P., Vachoux, C., Bermúdez-Humarán, L.G., Smirnova, N., Bergé, M., Sulpice, T., Lahtinen, S., et al. (2011). Intestinal mucosal adherence and translocation of commensal bacteria at the early onset of type 2 diabetes: molecular mechanisms and probiotic treatment. *EMBO Mol. Med.* 3, 559–572.
 47. Linh, H.T., Iwata, Y., Senda, Y., Sakai-Takemori, Y., Nakade, Y., Oshima, M., Nakagawa-Yoneda, S., Ogura, H., Sato, K., Minami, T., et al. (2022). Intestinal Bacterial Translocation Contributes to Diabetic Kidney Disease. *J. Am. Soc. Nephrol.* 33, 1105–1119.
 48. de Groot, P., Scheithauer, T., Bakker, G.J., Prodan, A., Levin, E., Khan, M.T., Herrema, H., Ackermans, M., Serlie, M.J.M., de Brauw, M., et al. (2020). Donor metabolic characteristics drive effects of faecal microbiota transplantation on recipient insulin sensitivity, energy expenditure and intestinal transit time. *Gut* 69, 502–512.
 49. Balaich, J., Estrella, M., Wu, G., Jeffrey, P.D., Biswas, A., Zhao, L., Korennykh, A., and Donia, M.S. (2021). The human microbiome encodes resistance to the antidiabetic drug acarbose. *Nature* 600, 110–115.
 50. Gacesa, R., Kurilshikov, A., Vich Vila, A., Sinha, T., Klaassen, M.A.Y., Bolte, L.A., Andreu-Sánchez, S., Chen, L., Collij, V., Hu, S., et al. (2022). Environmental factors shaping the gut microbiome in a Dutch population. *Nature* 604, 732–739.
 51. Asnicar, F., Berry, S.E., Valdes, A.M., Nguyen, L.H., Piccinno, G., Drew, D.A., Leeming, E., Gibson, R., Le Roy, C., Khatib, H.A., et al. (2021). Microbiome connections with host metabolism and habitual diet from 1,098 deeply phenotyped individuals. *Nat. Med.* 27, 321–332.
 52. Fassarella, M., Blaak, E.E., Penders, J., Nauta, A., Smidt, H., and Zoetendal, E.G. (2021). Gut microbiome stability and resilience: elucidating the response to perturbations in order to modulate gut health. *Gut* 70, 595–605.
 53. Price, N.D., Magis, A.T., Earls, J.C., Glusman, G., Levy, R., Lausted, C., McDonald, D.T., Kusebauch, U., Moss, C.L., Zhou, Y., et al. (2017). A wellness study of 108 individuals using personal, dense, dynamic data clouds. *Nat. Biotechnol.* 35, 747–756.
 54. Tebani, A., Gummesson, A., Zhong, W., Koistinen, I.S., Lakshminanth, T., Olsson, L.M., Boulund, F., Neiman, M., Stenlund, H., Hellström, C., et al. (2020). Integration of molecular profiles in a longitudinal wellness profiling cohort. *Nat. Commun.* 11, 4487.
 55. Olsson, L.M., Boulund, F., Nilsson, S., Khan, M.T., Gummesson, A., Fagerberg, L., Engstrand, L., Perkins, R., Uhlén, M., Bergström, G., et al. (2022). Dynamics of the normal gut microbiota: A longitudinal one-year population study in Sweden. *Cell Host Microbe* 30, 726–739.e3.
 56. Chen, L., Wang, D., Garmaeva, S., Kurilshikov, A., Vich Vila, A., Gacesa, R., Sinha, T., Lifelines Cohort Study, Segal, E., Weersma, R.K., et al. (2021). The long-term genetic stability and individual specificity of the human gut microbiome. *Cell* 184, 2302–2315.e2312.
 57. Li, J., Li, Y., Ivey, K.L., Wang, D.D., Wilkinson, J.E., Franke, A., Lee, K.H., Chan, A., Huttenhower, C., Hu, F.B., et al. (2022). Interplay between diet and gut microbiome, and circulating concentrations of trimethylamine N-oxide: findings from a longitudinal cohort of US men. *Gut* 71, 724–733.
 58. Zhou, W., Spoto, M., Hardy, R., Guan, C., Fleming, E., Larson, P.J., Brown, J.S., and Oh, J. (2020). Host-Specific Evolutionary and Transmission Dynamics Shape the Functional Diversification of *Staphylococcus epidermidis* in Human Skin. *Cell* 180, 454–470.e418.
 59. Costello, E.K., Lauber, C.L., Hamady, M., Fierer, N., Gordon, J.I., and Knight, R. (2009). Bacterial community variation in human body habitats across space and time. *Science* 326, 1694–1697.
 60. Larson, P.J., Chong, D., Fleming, E., and Oh, J. (2021). Challenges in Developing a Human Model System for Skin Microbiome Research. *J. Invest. Dermatol.* 141, 228–231.e4.

61. Selway, C.A., Sudarpha, J., and Weyrich, L.S. (2022). Moving beyond the gut microbiome: Combining systems biology and multi-site microbiome analyses to combat non-communicable diseases. *Med. Microecol.* *12*, 100052.
62. Oh, J., Byrd, A.L., Deming, C., Conlan, S., NISC Comparative Sequencing Program, Kong, H.H., and Segre, J.A. (2014). Biogeography and individuality shape function in the human skin metagenome. *Nature* *514*, 59–64.
63. Li, Z., Xia, J., Jiang, L., Tan, Y., An, Y., Zhu, X., Ruan, J., Chen, Z., Zhen, H., Ma, Y., et al. (2021). Characterization of the human skin resistome and identification of two microbiota cutotypes. *Microbiome* *9*, 47.
64. David, L.A., Materna, A.C., Friedman, J., Campos-Baptista, M.I., Blackburn, M.C., Perrotta, A., Erdman, S.E., and Alm, E.J. (2014). Host lifestyle affects human microbiota on daily timescales. *Genome Biol.* *15*, R89.
65. Oh, J., Freeman, A.F., NISC Comparative Sequencing Program, Park, M., Sokolic, R., Candotti, F., Holland, S.M., Segre, J.A., and Kong, H.H. (2013). The altered landscape of the human skin microbiome in patients with primary immunodeficiencies. *Genome Res.* *23*, 2103–2114.
66. Caporaso, J.G., Lauber, C.L., Costello, E.K., Berg-Lyons, D., Gonzalez, A., Stombaugh, J., Knights, D., Gajer, P., Ravel, J., Fierer, N., et al. (2011). Moving pictures of the human microbiome. *Genome Biol.* *12*, R50.
67. Olofsson, L.E., and Bäckhed, F. (2022). The Metabolic Role and Therapeutic Potential of the Microbiome. *Endocr. Rev.* *43*, 907–926.
68. Wozniak, J.M., Mills, R.H., Olson, J., Caldera, J.R., Sepich-Poore, G.D., Carrillo-Terrazas, M., Tsai, C.M., Vargas, F., Knight, R., Dorrestein, P.C., et al. (2020). Mortality Risk Profiling of *Staphylococcus aureus* Bacteremia by Multi-omic Serum Analysis Reveals Early Predictive and Pathogenic Signatures. *Cell* *182*, 1311–1327.e14.
69. Chen, R., Mias, G.I., Li-Pook-Than, J., Jiang, L., Lam, H.Y., Chen, R., Miriami, E., Karczewski, K.J., Hariharan, M., Dewey, F.E., et al. (2012). Personal omics profiling reveals dynamic molecular and medical phenotypes. *Cell* *148*, 1293–1307.
70. Zhou, W., Sailani, M.R., Contrepois, K., Zhou, Y., Ahadi, S., Leopold, S.R., Zhang, M.J., Rao, V., Avina, M., Mishra, T., et al. (2019). Longitudinal multi-omics of host-microbe dynamics in prediabetes. *Nature* *569*, 663–671.
71. Integrative HMP (iHMP) Research Network Consortium (2019). The Integrative Human Microbiome Project. *Nature* *569*, 641–648.
72. Callahan, B.J., McMurdie, P.J., and Holmes, S.P. (2017). Exact sequence variants should replace operational taxonomic units in marker-gene data analysis. *ISME J.* *11*, 2639–2643.
73. Johnson, J.S., Spakowicz, D.J., Hong, B.Y., Petersen, L.M., Demkowicz, P., Chen, L., Leopold, S.R., Hanson, B.M., Agresta, H.O., Gerstein, M., et al. (2019). Evaluation of 16S rRNA gene sequencing for species and strain-level microbiome analysis. *Nat. Commun.* *10*, 5029.
74. Schloss, P.D. (2021). Amplicon Sequence Variants Artificially Split Bacterial Genomes into Separate Clusters. *mSphere* *6*, e0019121.
75. Muniyappa, R., Lee, S., Chen, H., and Quon, M.J. (2008). Current approaches for assessing insulin sensitivity and resistance in vivo: advantages, limitations, and appropriate usage. *Am. J. Physiol. Endocrinol. Metab.* *294*, E15–E26.
76. Schüssler-Fiorenza Rose, S.M., Contrepois, K., Moneghetti, K.J., Zhou, W., Mishra, T., Mataraso, S., Dagan-Rosenfeld, O., Ganz, A.B., Dunn, J., Hornburg, D., et al. (2019). A longitudinal big data approach for precision health. *Nat. Med.* *25*, 792–804.
77. Arumugam, M., Raes, J., Pelletier, E., Le Paslier, D., Yamada, T., Mende, D.R., Fernandes, G.R., Tap, J., Bruls, T., Batto, J.M., et al. (2011). Enterotypes of the human gut microbiome. *Nature* *473*, 174–180.
78. Costea, P.I., Hildebrand, F., Arumugam, M., Bäckhed, F., Blaser, M.J., Bushman, F.D., de Vos, W.M., Ehrlich, S.D., Fraser, C.M., Hattori, M., et al. (2018). Enterotypes in the landscape of gut microbial community composition. *Nat. Microbiol.* *3*, 8–16.
79. Oh, J., Conlan, S., Polley, E.C., Segre, J.A., and Kong, H.H. (2012). Shifts in human skin and nares microbiota of healthy children and adults. *Genome Med.* *4*, 77.
80. García-López, M., Meier-Kolthoff, J.P., Tindall, B.J., Gronow, S., Woyke, T., Kyrpides, N.C., Hahnke, R.L., and Göker, M. (2019). Analysis of 1,000 Type-Strain Genomes Improves Taxonomic Classification of Bacteroidetes. *Front. Microbiol.* *10*, 2083.
81. Kilian, M., Chapple, I.L., Hannig, M., Marsh, P.D., Meuric, V., Pedersen, A.M., Tonetti, M.S., Wade, W.G., and Zaura, E. (2016). The oral microbiome - an update for oral healthcare professionals. *Br. Dent. J.* *221*, 657–666.
82. Aas, J.A., Paster, B.J., Stokes, L.N., Olsen, I., and Dewhirst, F.E. (2005). Defining the normal bacterial flora of the oral cavity. *J. Clin. Microbiol.* *43*, 5721–5732.
83. Mark Welch, J.L., Rossetti, B.J., Rieken, C.W., Dewhirst, F.E., and Borisy, G.G. (2016). Biogeography of a human oral microbiome at the micron scale. *Proc. Natl. Acad. Sci. USA* *113*, E791–E800.
84. Lahti, L., Salojärvi, J., Salonen, A., Scheffer, M., and de Vos, W.M. (2014). Tipping elements in the human intestinal ecosystem. *Nat. Commun.* *5*, 4344.
85. Sailani, M.R., Metwally, A.A., Zhou, W., Rose, S.M.S., Ahadi, S., Contrepois, K., Mishra, T., Zhang, M.J., Kidziński, L., Chu, T.J., and Snyder, M.P. (2020). Deep longitudinal multiomics profiling reveals two biological seasonal patterns in California. *Nat. Commun.* *11*, 4933.
86. Smits, S.A., Leach, J., Sonnenburg, E.D., Gonzalez, C.G., Lichtman, J.S., Reid, G., Knight, R., Manjuran, A., Changalucha, J., Elias, J.E., et al. (2017). Seasonal cycling in the gut microbiome of the Hadza hunter-gatherers of Tanzania. *Science* *357*, 802–806.
87. Koliada, A., Moseiko, V., Romanenko, M., Piven, L., Lushchak, O., Kryzhanovska, N., Guryanov, V., and Vaiserman, A. (2020). Seasonal variation in gut microbiota composition: cross-sectional evidence from Ukrainian population. *BMC Microbiol.* *20*, 100.
88. Wastyk, H.C., Fragiadakis, G.K., Perelman, D., Dahan, D., Merrill, B.D., Yu, F.B., Topf, M., Gonzalez, C.G., Van Treuren, W., Han, S., et al. (2021). Gut-microbiota-targeted diets modulate human immune status. *Cell* *184*, 4137–4153.e14.
89. Lancaster, S.M., Lee-McMullen, B., Abbott, C.W., Quijada, J.V., Hornburg, D., Park, H., Perelman, D., Peterson, D.J., Tang, M., Robinson, A., et al. (2022). Global, distinctive, and personal changes in molecular and microbial profiles by specific fibers in humans. *Cell Host Microbe* *30*, 848–862.e7.
90. Jiang, C., Wang, X., Li, X., Inlora, J., Wang, T., Liu, Q., and Snyder, M. (2018). Dynamic Human Environmental Exposome Revealed by Longitudinal Personal Monitoring. *Cell* *175*, 277–291.e31.
91. Fouladi, F., Bailey, M.J., Patterson, W.B., Sioda, M., Blakley, I.C., Fodor, A.A., Jones, R.B., Chen, Z., Kim, J.S., Lurmann, F., et al. (2020). Air pollution exposure is associated with the gut microbiome as revealed by shotgun metagenomic sequencing. *Environ. Int.* *138*, 105604.
92. Gao, P., Shen, X., Zhang, X., Jiang, C., Zhang, S., Zhou, X., Schüssler-Fiorenza Rose, S.M., and Snyder, M. (2022). Precision environmental health monitoring by longitudinal exposome and multi-omics profiling. *Genome Res.* *32*, 1199–1214.
93. Sunagawa, S., Schloissnig, S., Arumugam, M., Forslund, K., Mitreva, M., Tap, J., Zhu, A., Waller, A., Mende, D.R., Kultima, J.R., et al. (2013). Individuality and temporal stability of the human gut microbiome. *Cent. Asian J. Glob. Health* *2*, 120.
94. Mehta, R.S., Abu-Ali, G.S., Drew, D.A., Lloyd-Price, J., Subramanian, A., Lochhead, P., Joshi, A.D., Ivey, K.L., Khalili, H., Brown, G.T., et al. (2018). Stability of the human faecal microbiome in a cohort of adult men. *Nat. Microbiol.* *3*, 347–355.
95. Grice, E.A., Kong, H.H., Conlan, S., Deming, C.B., Davis, J., Young, A.C., Program, N.C.S., Bouffard, G.G., Blakesley, R.W., Murray, P.R., et al. (2009). Topographical and temporal diversity of the human skin microbiome. *Science* *324*, 1190–1192.

96. Gajer, P., Brotman, R.M., Bai, G., Sakamoto, J., Schütte, U.M., Zhong, X., Koenig, S.S., Fu, L., Ma, Z.S., Zhou, X., et al. (2012). Temporal dynamics of the human vaginal microbiota. *Sci. Transl. Med.* *4*, 132ra52.
97. Lemanceau, P., Blouin, M., Muller, D., and Moënne-Loccoz, Y. (2017). Let the Core Microbiota Be Functional. *Trends Plant Sci.* *22*, 583–595.
98. Priya, S., and Blekhan, R. (2019). Population dynamics of the human gut microbiome: change is the only constant. *Genome Biol.* *20*, 150.
99. Scapatucci, M., Marchetto, S., Nardi, A., Zoppelletto, M., and Bartolini, A. (2018). A case of necrotizing fasciitis caused by *Finegoldia magna* in a patient with type 2 diabetes mellitus. *Infez. Med.* *26*, 359–363.
100. Jneid, J., Cassir, N., Schuldiner, S., Jourdan, N., Sotto, A., Lavigne, J.P., and La Scola, B. (2018). Exploring the Microbiota of Diabetic Foot Infections With Culturomics. *Front. Cell. Infect. Microbiol.* *8*, 282.
101. Arencibia-Pérez, B., Benet-Muñoz, O., Roque-Castellano, C., and Marchena-Gómez, J. (2020). Gluteal Abscess due to *Finegoldia magna* in a Patient with Diabetes. *Actas Dermosifiliogr. Engl.* *111*, 527–528.
102. Castellanos, N., Nakanouchi, J., Yüzen, D.I., Fung, S., Fernandez, J.S., Barberis, C., Tuchscher, L., and Ramirez, M.S. (2019). A Study on *Acinetobacter baumannii* and *Staphylococcus aureus* Strains Recovered from the Same Infection Site of a Diabetic Patient. *Curr. Microbiol.* *76*, 842–847.
103. Perera, D., Kleinstein, S.E., Hanson, B., Hasturk, H., Eveloff, R., Freire, M., and Ramsey, M. (2021). Impaired host response and the presence of *Acinetobacter baumannii* in the serum microbiome of type-II diabetic patients. *iScience* *24*, 101941.
104. Leung, C.H., and Liu, C.P. (2019). Diabetic status and the relationship of blood glucose to mortality in adults with carbapenem-resistant *Acinetobacter baumannii* complex bacteremia. *J. Microbiol. Immunol. Infect.* *52*, 654–662.
105. Henig, O., Pogue, J.M., Martin, E., Hayat, U., Ja'ara, M., Kilgore, P.E., Cha, R., Dhar, S., and Kaye, K.S. (2020). The Impact of Multidrug-Resistant Organisms on Outcomes in Patients With Diabetic Foot Infections. *Open Forum Infect. Dis.* *7*, ofaa161.
106. Min, K.R., Galvis, A., Baquerizo Nole, K.L., Sinha, R., Clarke, J., Kirsner, R.S., and Ajdic, D. (2020). Association between baseline abundance of *Peptoniphilus*, a Gram-positive anaerobic coccus, and wound healing outcomes of DFUs. *PLoS One* *15*, e0227006.
107. Smith, K., Collier, A., Townsend, E.M., O'Donnell, L.E., Bal, A.M., Butcher, J., Mackay, W.G., Ramage, G., and Williams, C. (2016). One step closer to understanding the role of bacteria in diabetic foot ulcers: characterising the microbiome of ulcers. *BMC Microbiol.* *16*, 54.
108. Brown, K., Church, D., Lynch, T., and Gregson, D. (2014). Bloodstream infections due to *Peptoniphilus* spp.: report of 15 cases. *Clin. Microbiol. Infect.* *20*, O857–O860.
109. iMSMS Consortium. Electronic address:sergio.baranzini@ucsf.edu, and iMSMS Consortium (2022). Gut microbiome of multiple sclerosis patients and paired household healthy controls reveal associations with disease risk and course. *Cell* *185*, 3467–3486.e16.
110. Zhao, S., Lieberman, T.D., Poyet, M., Kauffman, K.M., Gibbons, S.M., Groussin, M., Xavier, R.J., and Alm, E.J. (2019). Adaptive Evolution within Gut Microbiomes of Healthy People. *Cell Host Microbe* *25*, 656–667.e8.
111. Carrow, H.C., Batachari, L.E., and Chu, H. (2020). Strain diversity in the microbiome: Lessons from *Bacteroides fragilis*. *PLoS Pathog.* *16*, e1009056.
112. Lee, S.M., Donaldson, G.P., Mikulski, Z., Boyajian, S., Ley, K., and Mazmanian, S.K. (2013). Bacterial colonization factors control specificity and stability of the gut microbiota. *Nature* *501*, 426–429.
113. Rothschild, D., Weissbrod, O., Barkan, E., Kurilshikov, A., Korem, T., Zeevi, D., Costea, P.I., Godneva, A., Kalka, I.N., Bar, N., et al. (2018). Environment dominates over host genetics in shaping human gut microbiota. *Nature* *555*, 210–215.
114. Kort, R., Caspers, M., van de Graaf, A., van Egmond, W., Keijsers, B., and Roeselers, G. (2014). Shaping the oral microbiota through intimate kissing. *Microbiome* *2*, 41.
115. Rocha, J., Henriques, I., Gomila, M., and Manaia, C.M. (2022). Common and distinctive genomic features of *Klebsiella pneumoniae* thriving in the natural environment or in clinical settings. *Sci. Rep.* *12*, 10441.
116. Musher, D.M. (1996). *Haemophilus* Species. In *Medical Microbiology* (University of Texas Medical Branch at Galveston).
117. Vieira-Silva, S., Falony, G., Belda, E., Nielsen, T., Aron-Wisniewsky, J., Chakaroun, R., Forslund, S.K., Assmann, K., Valles-Colomer, M., Nguyen, T.T.D., et al. (2020). Statin therapy is associated with lower prevalence of gut microbiota dysbiosis. *Nature* *587*, 310–315.
118. Byrd, A.L., Liu, M., Fujimura, K.E., Lyalina, S., Nagarkar, D.R., Charbit, B., Bergstedt, J., Patin, E., Harrison, O.J., Quintana-Murci, L., et al. (2021). Gut microbiome stability and dynamics in healthy donors and patients with non-gastrointestinal cancers. *J. Exp. Med.* *218*, e20200606.
119. Byrd, A.L., Belkaid, Y., and Segre, J.A. (2018). The human skin microbiome. *Nat. Rev. Microbiol.* *16*, 143–155.
120. Flores, G.E., Caporaso, J.G., Henley, J.B., Rideout, J.R., Domogala, D., Chase, J., Leff, J.W., Vázquez-Baeza, Y., Gonzalez, A., Knight, R., et al. (2014). Temporal variability is a personalized feature of the human microbiome. *Genome Biol.* *15*, 531.
121. Ontiveros, V.J., Capitán, J.A., Casamayor, E.O., and Alonso, D. (2021). The characteristic time of ecological communities. *Ecology* *102*, e03247.
122. Real, R., and Vargas, J.M. (1996). The Probabilistic Basis of Jaccard's Index of Similarity. *Syst. Biol.* *45*, 380–385.
123. Li, S.S., Zhu, A., Benes, V., Costea, P.I., Hercog, R., Hildebrand, F., Huerta-Cepas, J., Nieuwdorp, M., Salojärvi, J., Voigt, A.Y., et al. (2016). Durable coexistence of donor and recipient strains after fecal microbiota transplantation. *Science* *352*, 586–589.
124. Russell, B.J., Brown, S.D., Siguenza, N., Mai, I., Saran, A.R., Lingaraju, A., Maissy, E.S., Dantas Machado, A.C., Pinto, A.F.M., Sanchez, C., et al. (2022). Intestinal transgene delivery with native *E. coli* chassis allows persistent physiological changes. *Cell* *185*, 3263–3277.e15.
125. Bartley, J.M., Zhou, X., Kuchel, G.A., Weinstock, G.M., and Haynes, L. (2017). Impact of Age, Caloric Restriction, and Influenza Infection on Mouse Gut Microbiome: An Exploratory Study of the Role of Age-Related Microbiome Changes on Influenza Responses. *Front. Immunol.* *8*, 1164.
126. Czerkinsky, C., Prince, S.J., Michalek, S.M., Jackson, S., Russell, M.W., Moldoveanu, Z., McGhee, J.R., and Mestecky, J. (1987). IgA antibody-producing cells in peripheral blood after antigen ingestion: evidence for a common mucosal immune system in humans. *Proc. Natl. Acad. Sci. USA* *84*, 2449–2453.
127. Winer, D.A., Luck, H., Tsai, S., and Winer, S. (2016). The Intestinal Immune System in Obesity and Insulin Resistance. *Cell Metab.* *23*, 413–426.
128. Wang, J., Li, F., Wei, H., Lian, Z.X., Sun, R., and Tian, Z. (2014). Respiratory influenza virus infection induces intestinal immune injury via microbiota-mediated Th17 cell-dependent inflammation. *J. Exp. Med.* *211*, 2397–2410.
129. Oh, J., and Unutmaz, D. (2019). Immune cells for microbiota surveillance. *Science* *366*, 419–420.
130. Zhao, L., Zhang, F., Ding, X., Wu, G., Lam, Y.Y., Wang, X., Fu, H., Xue, X., Lu, C., Ma, J., et al. (2018). Gut bacteria selectively promoted by dietary fibers alleviate type 2 diabetes. *Science* *359*, 1151–1156.
131. Wu, G., Zhao, N., Zhang, C., Lam, Y.Y., and Zhao, L. (2021). Guild-based analysis for understanding gut microbiome in human health and diseases. *Genome Med.* *13*, 22.
132. Guo, M., Wu, G., Tan, Y., Li, Y., Jin, X., Qi, W., Guo, X., Zhang, C., Zhu, Z., and Zhao, L. (2023). Guild-Level Microbiome Signature Associated with COVID-19 Severity and Prognosis. *mBio* *14*, e0351922.
133. Chen, X., Li, P., Liu, M., Zheng, H., He, Y., Chen, M.X., Tang, W., Yue, X., Huang, Y., Zhuang, L., et al. (2020). Gut dysbiosis induces the development of pre-eclampsia through bacterial translocation. *Gut* *69*, 513–522.

134. Marchetti, G., Tincati, C., and Silvestri, G. (2013). Microbial translocation in the pathogenesis of HIV infection and AIDS. *Clin. Microbiol. Rev.* 26, 2–18.
135. Qin, N., Yang, F., Li, A., Prifti, E., Chen, Y., Shao, L., Guo, J., Le Chatelier, E., Yao, J., Wu, L., et al. (2014). Alterations of the human gut microbiome in liver cirrhosis. *Nature* 513, 59–64.
136. Schloissnig, S., Arumugam, M., Sunagawa, S., Mitreva, M., Tap, J., Zhu, A., Waller, A., Mende, D.R., Kultima, J.R., Martin, J., et al. (2013). Genomic variation landscape of the human gut microbiome. *Nature* 493, 45–50.
137. Lynn, D.J., Benson, S.C., Lynn, M.A., and Pulendran, B. (2022). Modulation of immune responses to vaccination by the microbiota: implications and potential mechanisms. *Nat. Rev. Immunol.* 22, 33–46.
138. Müller, M., and Betlejewski, S. (2003). Nasal mucosa in patients with diabetes mellitus. *Otolaryngol. Pol.* 57, 361–364.
139. Lee, T.K., Jeon, Y.J., and Jung, S.J. (2021). Bi-directional association between allergic rhinitis and diabetes mellitus from the national representative data of South Korea. *Sci. Rep.* 11, 4344.
140. Nam, J.S., Roh, Y.H., Kim, J., Chang, S.W., Ha, J.G., Park, J.J., Fahad, W.A., Yoon, J.H., Kim, C.H., and Cho, H.J. (2022). Association between diabetes mellitus and chronic rhinosinusitis with nasal polyps: A population-based cross-sectional study. *Clin. Otolaryngol.* 47, 167–173.
141. Schirmer, M., Smeekens, S.P., Vlamakis, H., Jaeger, M., Oosting, M., Franzosa, E.A., Ter Horst, R., Jansen, T., Jacobs, L., Bonder, M.J., et al. (2016). Linking the Human Gut Microbiome to Inflammatory Cytokine Production Capacity. *Cell* 167, 1125–1136.e8.
142. Geva-Zatorsky, N., Sefik, E., Kua, L., Pasman, L., Tan, T.G., Ortiz-Lopez, A., Yanortsang, T.B., Yang, L., Jupp, R., Mathis, D., et al. (2017). Mining the Human Gut Microbiota for Immunomodulatory Organisms. *Cell* 168, 928–943.e11.
143. Mendes, V., Galvão, I., and Vieira, A.T. (2019). Mechanisms by Which the Gut Microbiota Influences Cytokine Production and Modulates Host Inflammatory Responses. *J. Interferon Cytokine Res.* 39, 393–409.
144. Bolte, L.A., Vich Vila, A., Imhann, F., Collij, V., Gacesa, R., Peters, V., Wijmenga, C., Kurilshikov, A., Campmans-Kuijpers, M.J.E., Fu, J., et al. (2021). Long-term dietary patterns are associated with pro-inflammatory and anti-inflammatory features of the gut microbiome. *Gut* 70, 1287–1298.
145. Zhou, X., Johnson, J.S., Spakowicz, D., Zhou, W., Zhou, Y., Sodergren, E., Snyder, M., and Weinstock, G.M. (2020). Longitudinal Analysis of Serum Cytokine Levels and Gut Microbial Abundance Links IL-17/IL-22 With Clostridia and Insulin Sensitivity in Humans. *Diabetes* 69, 1833–1842.
146. Lloyd-Price, J., Mahurkar, A., Rahnavard, G., Crabtree, J., Orvis, J., Hall, A.B., Brady, A., Creasy, H.H., McCracken, C., Giglio, M.G., et al. (2017). Strains, functions and dynamics in the expanded Human Microbiome Project. *Nature* 550, 61–66.
147. Turnbaugh, P.J., Hamady, M., Yatsunenkov, T., Cantarel, B.L., Duncan, A., Ley, R.E., Sogin, M.L., Jones, W.J., Roe, B.A., Affourtit, J.P., et al. (2009). A core gut microbiome in obese and lean twins. *Nature* 457, 480–484.
148. Somineni, H.K., Weitzner, J.H., Venkateswaran, S., Dodd, A., Prince, J., Karikaran, A., Sauer, C.G., Abramowicz, S., Zwick, M.E., Cutler, D.J., et al. (2021). Site- and Taxa-Specific Disease-Associated Oral Microbial Structures Distinguish Inflammatory Bowel Diseases. *Inflamm. Bowel Dis.* 27, 1889–1900.
149. Gao, Z., Tseng, C.H., Strober, B.E., Pei, Z., and Blaser, M.J. (2008). Substantial alterations of the cutaneous bacterial biota in psoriatic lesions. *PLoS One* 3, e2719.
150. Shin, N.R., Whon, T.W., and Bae, J.W. (2015). Proteobacteria: microbial signature of dysbiosis in gut microbiota. *Trends Biotechnol.* 33, 496–503.
151. Bradley, P.H., and Pollard, K.S. (2017). Proteobacteria explain significant functional variability in the human gut microbiome. *Microbiome* 5, 36.
152. d’Hennezel, E., Abubucker, S., Murphy, L.O., and Cullen, T.W. (2017). Total Lipopolysaccharide from the Human Gut Microbiome Silences Toll-Like Receptor Signaling. *mSystems* 2, e00046-e00017.
153. Pither, M.D., Illiano, A., Pagliuca, C., Jacobson, A., Mantova, G., Stornaiuolo, A., Colicchio, R., Vitiello, M., Pinto, G., and Silipo, A. (2022). *Bacteroides thetaiotaomicron* rough-type lipopolysaccharide: The chemical structure and the immunological activity. *Carbohydr. Polym.* 297, 120040.
154. Vatanen, T., Kostic, A.D., d’Hennezel, E., Siljander, H., Franzosa, E.A., Yassour, M., Kolde, R., Vlamakis, H., Arthur, T.D., Hämmäläinen, A.M., et al. (2016). Variation in Microbiome LPS Immunogenicity Contributes to Autoimmunity in Humans. *Cell* 165, 842–853.
155. Deriu, E., Boxx, G.M., He, X., Pan, C., Benavidez, S.D., Cen, L., Rozengurt, N., Shi, W., and Cheng, G. (2016). Influenza Virus Affects Intestinal Microbiota and Secondary Salmonella Infection in the Gut through Type I Interferons. *PLoS Pathog.* 12, e1005572.
156. Winter, S.E., and Bäuml, A.J. (2014). Why related bacterial species bloom simultaneously in the gut: principles underlying the ‘Like will to like’ concept. *Cell. Microbiol.* 16, 179–184.
157. Scales, B.S., Dickson, R.P., and Huffnagle, G.B. (2016). A tale of two sites: how inflammation can reshape the microbiomes of the gut and lungs. *J. Leukoc. Biol.* 100, 943–950.
158. Turnbaugh, P.J., Ley, R.E., Mahowald, M.A., Magrini, V., Mardis, E.R., and Gordon, J.I. (2006). An obesity-associated gut microbiome with increased capacity for energy harvest. *Nature* 444, 1027–1031.
159. Maruvada, P., Leone, V., Kaplan, L.M., and Chang, E.B. (2017). The Human Microbiome and Obesity: Moving beyond Associations. *Cell Host Microbe* 22, 589–599.
160. Yang, D., Johnson, J., Zhou, X., Deych, E., Shands, B., Hanson, B., Sodergren, E., Weinstock, G., and Shannon, W.D. (2019). New statistical method identifies cytokines that distinguish stool microbiomes. *Sci. Rep.* 9, 20082.
161. Mallick, H., Franzosa, E.A., McLver, L.J., Banerjee, S., Sirota-Madi, A., Kostic, A.D., Clish, C.B., Vlamakis, H., Xavier, R.J., and Huttenhower, C. (2019). Predictive metabolomic profiling of microbial communities using amplicon or metagenomic sequences. *Nat. Commun.* 10, 3136.
162. Park, S.Y., Rao, C., Coyte, K.Z., Kuziel, G.A., Zhang, Y., Huang, W., Franzosa, E.A., Weng, J.K., Huttenhower, C., and Rakoff-Nahoum, S. (2022). Strain-level fitness in the gut microbiome is an emergent property of glycans and a single metabolite. *Cell* 185, 513–529.e21. e521.
163. Petersen, L.M., Bautista, E.J., Nguyen, H., Hanson, B.M., Chen, L., Lek, S.H., Sodergren, E., and Weinstock, G.M. (2017). Community characteristics of the gut microbiomes of competitive cyclists. *Microbiome* 5, 98.
164. Patra, A.K., and Yu, Z. (2022). Genomic Insights into the Distribution of Peptidases and Proteolytic Capacity among *Prevotella* and *Paraprevotella* Species. *Microbiol. Spectr.* 10, e0218521.
165. Lamichhane, S., Sen, P., Alves, M.A., Ribeiro, H.C., Raunioemi, P., Hyötyläinen, T., and Orešić, M. (2021). Linking Gut Microbiome and Lipid Metabolism: Moving beyond Associations. *Metabolites* 11, 55.
166. Flint, H.J., and Duncan, S. (2014). *Bacteroides* and *Prevotella*. In *Encyclopedia of Food Microbiology*, Second Edition (Elsevier Inc.).
167. Visconti, A., Le Roy, C.I., Rosa, F., Rossi, N., Martin, T.C., Mohney, R.P., Li, W., de Rinaldis, E., Bell, J.T., Venter, J.C., et al. (2019). Interplay between the human gut microbiome and host metabolism. *Nat. Commun.* 10, 4505.
168. Diener, C., Dai, C.L., Wilmanski, T., Baloni, P., Smith, B., Rappaport, N., Hood, L., Magis, A.T., and Gibbons, S.M. (2022). Genome-microbiome interplay provides insight into the determinants of the human blood metabolome. *Nat. Metab.* 4, 1560–1572.
169. Song, B.-J., Akbar, M., Jo, I., Hardwick, J.P., and Abdelmegeed, M.A. (2015). Translational implications of the alcohol-metabolizing enzymes, including cytochrome P450-2E1, in Alcoholic and Nonalcoholic Liver Disease. *Adv. Pharmacol.* 74, 303–372.

170. Engen, P.A., Green, S.J., Voigt, R.M., Forsyth, C.B., and Keshavarzian, A. (2015). The Gastrointestinal Microbiome: Alcohol Effects on the Composition of Intestinal Microbiota. *Alcohol Res.* *37*, 223–236.
171. Kosnicki, K.L., Penprase, J.C., Cintora, P., Torres, P.J., Harris, G.L., Brasser, S.M., and Kelley, S.T. (2019). Effects of moderate, voluntary ethanol consumption on the rat and human gut microbiome. *Addict. Biol.* *24*, 617–630.
172. Fan, X., Peters, B.A., Jacobs, E.J., Gapstur, S.M., Purdue, M.P., Freedman, N.D., Alekseyenko, A.V., Wu, J., Yang, L., Pei, Z., et al. (2018). Drinking alcohol is associated with variation in the human oral microbiome in a large study of American adults. *Microbiome* *6*, 59.
173. Yokoyama, S., Takeuchi, K., Shibata, Y., Kageyama, S., Matsumi, R., Takeshita, T., and Yamashita, Y. (2018). Characterization of oral microbiota and acetaldehyde production. *J. Oral Microbiol.* *10*, 1492316.
174. Tagaino, R., Washio, J., Abiko, Y., Tanda, N., Sasaki, K., and Takahashi, N. (2019). Metabolic property of acetaldehyde production from ethanol and glucose by oral *Streptococcus* and *Neisseria*. *Sci. Rep.* *9*, 10446.
175. Yuan, J., Chen, C., Cui, J., Lu, J., Yan, C., Wei, X., Zhao, X., Li, N., Li, S., Xue, G., et al. (2019). Fatty Liver Disease Caused by High-Alcohol-Producing *Klebsiella pneumoniae*. *Cell Metab.* *30*, 675–688.e677.
176. Li, N.N., Li, W., Feng, J.X., Zhang, W.W., Zhang, R., Du, S.H., Liu, S.Y., Xue, G.H., Yan, C., Cui, J.H., et al. (2021). High alcohol-producing *Klebsiella pneumoniae* causes fatty liver disease through 2,3-butanediol fermentation pathway in vivo. *Gut Microbes* *13*, 1979883.
177. Sakamoto, M., Ikeyama, N., Yuki, M., and Ohkuma, M. (2018). Draft Genome Sequence of *Faecalimonas umbilicata* JCM 30896(T), an Acetate-Producing Bacterium Isolated from Human Feces. *Microbiol. Resour. Annu.* *7*. e01091-e01018.
178. Spector, M. (2009). Metabolism, central (intermediary). In *Encyclopedia of Microbiology* (Elsevier Inc.).
179. Tsuruya, A., Kuwahara, A., Saito, Y., Yamaguchi, H., Tsubo, T., Suga, S., Inai, M., Aoki, Y., Takahashi, S., Tsutsumi, E., et al. (2016). Ecophysiological consequences of alcoholism on human gut microbiota: implications for ethanol-related pathogenesis of colon cancer. *Sci. Rep.* *6*, 27923.
180. Petersen, C., Bell, R., Klag, K.A., Lee, S.H., Soto, R., Ghazaryan, A., Buhrke, K., Ekiz, H.A., Ost, K.S., Boudina, S., et al. (2019). T cell-mediated regulation of the microbiota protects against obesity. *Science* *365*, eaat9351.
181. Lin, Y.C., Lin, H.F., Wu, C.C., Chen, C.L., and Ni, Y.H. (2022). Pathogenic effects of *Desulfovibrio* in the gut on fatty liver in diet-induced obese mice and children with obesity. *J. Gastroenterol.* *57*, 913–925.
182. Le Chatelier, E., Nielsen, T., Qin, J., Prifti, E., Hildebrand, F., Falony, G., Almeida, M., Arumugam, M., Batto, J.M., Kennedy, S., et al. (2013). Richness of human gut microbiome correlates with metabolic markers. *Nature* *500*, 541–546.
183. Wilmanski, T., Rappaport, N., Earls, J.C., Magis, A.T., Manor, O., Lovejoy, J., Omenn, G.S., Hood, L., Gibbons, S.M., and Price, N.D. (2019). Blood metabolome predicts gut microbiome alpha-diversity in humans. *Nat. Biotechnol.* *37*, 1217–1228.
184. Passmore, I.J., Letertre, M.P.M., Preston, M.D., Bianconi, I., Harrison, M.A., Nasher, F., Kaur, H., Hong, H.A., Baines, S.D., Cutting, S.M., et al. (2018). Para-cresol production by *Clostridium difficile* affects microbial diversity and membrane integrity of Gram-negative bacteria. *PLoS Pathog.* *14*, e1007191.
185. Koppe, L., Alix, P.M., Croze, M.L., Chambert, S., Vanholder, R., Glorieux, G., Fouque, D., and Soulage, C.O. (2017). p-Cresyl glucuronide is a major metabolite of p-cresol in mouse: in contrast to p-cresyl sulphate, p-cresyl glucuronide fails to promote insulin resistance. *Nephrol. Dial. Transplant.* *32*, 2000–2009.
186. Kasahara, K., Krautkramer, K.A., Org, E., Romano, K.A., Kerby, R.L., Vivas, E.I., Mehrabian, M., Denu, J.M., Bäckhed, F., Luskis, A.J., and Rey, F.E. (2018). Interactions between *Roseburia intestinalis* and diet modulate atherogenesis in a murine model. *Nat. Microbiol.* *3*, 1461–1471.
187. La Rosa, S.L., Leth, M.L., Michalak, L., Hansen, M.E., Pudlo, N.A., Glowacki, R., Pereira, G., Workman, C.T., Arntzen, M.Ø., Pope, P.B., et al. (2019). The human gut Firmicute *Roseburia intestinalis* is a primary degrader of dietary beta-mannans. *Nat. Commun.* *10*, 905.
188. Nie, K., Ma, K., Luo, W., Shen, Z., Yang, Z., Xiao, M., Tong, T., Yang, Y., and Wang, X. (2021). *Roseburia intestinalis*: A Beneficial Gut Organism From the Discoveries in Genus and Species. *Front. Cell. Infect. Microbiol.* *11*, 757718.
189. VanderWeele, T.J. (2016). *Mediation Analysis: A Practitioner's Guide*. *Annu. Rev. Public Health* *37*, 17–32.
190. Jiang, Z., Zhuo, L.B., He, Y., Fu, Y., Shen, L., Xu, F., Gou, W., Miao, Z., Shuai, M., Liang, Y., et al. (2022). The gut microbiota-bile acid axis links the positive association between chronic insomnia and cardiometabolic diseases. *Nat. Commun.* *13*, 3002.
191. Takeuchi, T., Kubota, T., Nakanishi, Y., Tsugawa, H., Suda, W., Kwon, A.T., Yazaki, J., Ikeda, K., Nemoto, S., Mochizuki, Y., et al. (2023). Gut microbial carbohydrate metabolism contributes to insulin resistance. *Nature* *621*, 389–395.
192. Lee, H., Cashin, A.G., Lamb, S.E., Hopewell, S., Vansteelandt, S., VanderWeele, T.J., MacKinnon, D.P., Mansell, G., Collins, G.S., Golub, R.M., et al. (2021). A Guideline for Reporting Mediation Analyses of Randomized Trials and Observational Studies: The AGRReMA Statement. *JAMA* *326*, 1045–1056.
193. Demmer, R.T., Breskin, A., Rosenbaum, M., Zuk, A., LeDuc, C., Leibel, R., Paster, B., Desvarieux, M., Jacobs, D.R., Jr., and Papapanou, P.N. (2017). The subgingival microbiome, systemic inflammation and insulin resistance: The Oral Infections, Glucose Intolerance and Insulin Resistance Study. *J. Clin. Periodontol.* *44*, 255–265.
194. Demmer, R.T., Squillaro, A., Papapanou, P.N., Rosenbaum, M., Friedewald, W.T., Jacobs, D.R., Jr., and Desvarieux, M. (2012). Periodontal infection, systemic inflammation, and insulin resistance: results from the continuous National Health and Nutrition Examination Survey (NHANES) 1999–2004. *Diabetes Care* *35*, 2235–2242.
195. Li, X., Kolltveit, K.M., Tronstad, L., and Olsen, I. (2000). Systemic diseases caused by oral infection. *Clin. Microbiol. Rev.* *13*, 547–558.
196. Ďásková, N., Modos, I., Krbcová, M., Kuzma, M., Pelantová, H., Hradecký, J., Heczková, M., Bratová, M., Videňská, P., Šplichalová, P., et al. (2023). Multi-omics signatures in new-onset diabetes predict metabolic response to dietary inulin: findings from an observational study followed by an interventional trial. *Nutr. Diabetes* *13*, 7.
197. Berglund, L., Berne, C., Svärdsudd, K., Garmo, H., Melhus, H., and Zethelius, B. (2012). Seasonal variations of insulin sensitivity from a euglycemic insulin clamp in elderly men. *Ups. J. Med. Sci.* *117*, 35–40.
198. Chen, S.H., Chuang, S.Y., Lin, K.C., Tsai, S.T., and Chou, P. (2008). Community-based study on summer-winter difference in insulin resistance in Kin-Chen, Kinmen, Taiwan. *J. Chin. Med. Assoc.* *71*, 619–627.
199. Wilmanski, T., Kornilov, S.A., Diener, C., Conomos, M.P., Lovejoy, J.C., Sebastiani, P., Orwoll, E.S., Hood, L., Price, N.D., Rappaport, N., et al. (2022). Heterogeneity in statin responses explained by variation in the human gut microbiome. *Med.* *3*, 388–405.e6.
200. Ding, T., and Schloss, P.D. (2014). Dynamics and associations of microbial community types across the human body. *Nature* *509*, 357–360.
201. Adler, C.J., Dobney, K., Weyrich, L.S., Kaidonis, J., Walker, A.W., Haak, W., Bradshaw, C.J., Townsend, G., Sołtysiak, A., Ait, K.W., et al. (2013). Sequencing ancient calcified dental plaque shows changes in oral microbiota with dietary shifts of the Neolithic and Industrial revolutions. *Nat. Genet.* *45*, 450–455.e451.
202. Asangba, A.E., Mugisha, L., Rukundo, J., Lewis, R.J., Halajian, A., Cortés-Ortiz, L., Junge, R.E., Irwin, M.T., Karlson, J., Perkin, A., et al. (2022). Large Comparative Analyses of Primate Body Site Microbiomes Indicate that the Oral Microbiome Is Unique among All Body Sites and Conserved among Nonhuman Primates. *Microbiol. Spectr.* *10*, e0164321.

203. Lv, L., Jiang, H., Yan, R., Xu, D., Wang, K., Wang, Q., Chen, X., and Li, L. (2021). The Salivary Microbiota, Cytokines, and Metabolome in Patients with Ankylosing Spondylitis Are Altered and More Proinflammatory than Those in Healthy Controls. *mSystems* 6, e0117320.
204. Elias, A.E., McBain, A.J., and O'Neill, C.A. (2021). The role of the skin microbiota in the modulation of cutaneous inflammation—Lessons from the gut. *Exp. Dermatol.* 30, 1509–1516.
205. Harris-Tryon, T.A., and Grice, E.A. (2022). Microbiota and maintenance of skin barrier function. *Science* 376, 940–945.
206. Wu, H., and Ballantyne, C.M. (2020). Metabolic Inflammation and Insulin Resistance in Obesity. *Circ. Res.* 126, 1549–1564.
207. Vujkovic-Cvijin, I., Sklar, J., Jiang, L., Natarajan, L., Knight, R., and Belkaid, Y. (2020). Host variables confound gut microbiota studies of human disease. *Nature* 587, 448–454.
208. Zhu, L., Baker, S.S., Gill, C., Liu, W., Alkhoury, R., Baker, R.D., and Gill, S.R. (2013). Characterization of gut microbiomes in nonalcoholic steatohepatitis (NASH) patients: a connection between endogenous alcohol and NASH. *Hepatology* 57, 601–609.
209. Wu, G.D., Chen, J., Hoffmann, C., Bittinger, K., Chen, Y.Y., Keilbaugh, S.A., Bewtra, M., Knights, D., Walters, W.A., Knight, R., et al. (2011). Linking long-term dietary patterns with gut microbial enterotypes. *Science* 334, 105–108.
210. Gribbon, E.M., Cunliffe, W.J., and Holland, K.T. (1993). Interaction of *Propionibacterium acnes* with skin lipids in vitro. *J. Gen. Microbiol.* 139, 1745–1751.
211. Mayslich, C., Grange, P.A., and Dupin, N. (2021). *Cutibacterium acnes* as an Opportunistic Pathogen: An Update of Its Virulence-Associated Factors. *Microorganisms* 9, 303.
212. Brown, E.M., Ke, X., Hitchcock, D., Jeanfavre, S., Avila-Pacheco, J., Nakata, T., Arthur, T.D., Fornelos, N., Heim, C., Franzosa, E.A., et al. (2019). *Bacteroides*-Derived Sphingolipids Are Critical for Maintaining Intestinal Homeostasis and Symbiosis. *Cell Host Microbe* 25, 668–680.e7.
213. Kenny, D.J., Plichta, D.R., Shungin, D., Koppel, N., Hall, A.B., Fu, B., Vasani, R.S., Shaw, S.Y., Vlamakis, H., Balskus, E.P., and Xavier, R.J. (2020). Cholesterol Metabolism by Uncultured Human Gut Bacteria Influences Host Cholesterol Level. *Cell Host Microbe* 28, 245–257.e6.
214. Cryan, J.F., and Mazmanian, S.K. (2022). Microbiota-brain axis: Context and causality. *Science* 376, 938–939.
215. Needham, B.D., Funabashi, M., Adame, M.D., Wang, Z., Boktor, J.C., Haney, J., Wu, W.L., Rabut, C., Ladinsky, M.S., Hwang, S.J., et al. (2022). A gut-derived metabolite alters brain activity and anxiety behaviour in mice. *Nature* 602, 647–653.
216. Budden, K.F., Gellatly, S.L., Wood, D.L., Cooper, M.A., Morrison, M., Hugenholz, P., and Hansbro, P.M. (2017). Emerging pathogenic links between microbiota and the gut-lung axis. *Nat. Rev. Microbiol.* 15, 55–63.
217. Marsland, B.J., Trompette, A., and Gollwitzer, E.S. (2015). The Gut-Lung Axis in Respiratory Disease. *Ann. Am. Thorac. Soc.* 12, S150–S156.
218. Atarashi, K., Suda, W., Luo, C., Kawaguchi, T., Motoo, I., Narushima, S., Kiguchi, Y., Yasuma, K., Watanabe, E., Tanoue, T., et al. (2017). Ectopic colonization of oral bacteria in the intestine drives TH1 cell induction and inflammation. *Science* 358, 359–365.
219. Samuelson, D.R., Shellito, J.E., Maffei, V.J., Tague, E.D., Campagna, S.R., Blanchard, E.E., Luo, M., Taylor, C.M., Ronis, M.J.J., Molina, P.E., et al. (2017). Alcohol-associated intestinal dysbiosis impairs pulmonary host defense against *Klebsiella pneumoniae*. *PLoS Pathog.* 13, e1006426.
220. Shellito, J.E., Quan Zheng, M., Ye, P., Ruan, S., Shean, M.K., and Kolls, J. (2001). Effect of alcohol consumption on host release of interleukin-17 during pulmonary infection with *Klebsiella pneumoniae*. *Alcohol. Clin. Exp. Res.* 25, 872–881.
221. Samuelson, D.R., Gu, M., Shellito, J.E., Molina, P.E., Taylor, C.M., Luo, M., and Welsh, D.A. (2021). Pulmonary immune cell trafficking promotes host defense against alcohol-associated *Klebsiella pneumoniae*. *Commun. Biol.* 4, 997.
222. Louis, P., and Flint, H.J. (2009). Diversity, metabolism and microbial ecology of butyrate-producing bacteria from the human large intestine. *FEMS Microbiol. Lett.* 294, 1–8.
223. Sakamoto, M., Iino, T., Yuki, M., and Ohkuma, M. (2018). *Lawsonibacter asaccharolyticus* gen. nov., sp. nov., a butyrate-producing bacterium isolated from human faeces. *Int. J. Syst. Evol. Microbiol.* 68, 2074–2081.
224. Kläring, K., Hanske, L., Bui, N., Charrier, C., Blaut, M., Haller, D., Plugge, C.M., and Clavel, T. (2013). *Intestinimonas butyriciproducens* gen. nov., sp. nov., a butyrate-producing bacterium from the mouse intestine. *Int. J. Syst. Evol. Microbiol.* 63, 4606–4612.
225. Bui, T.P.N., Troise, A.D., Nijssse, B., Roviello, G.N., Fogliano, V., and de Vos, W.M. (2020). *Intestinimonas*-like bacteria are important butyrate producers that utilize *Nε*-fructosyllysine and lysine in formula-fed infants and adults. *J. Funct. Foods* 70, 103974.
226. Greene, J.A., and Keohen, G.F. (1943). Insulin resistance due to infection in diabetes mellitus in man. *J. Am. Med. Assoc.* 121, 173–176.
227. Šestan, M., Marinović, S., Kavazović, I., Cekinović, Đ., Wuest, S., Turk Wensveen, T., Brzić, I., Jonjić, S., Konrad, D., Wensveen, F.M., and Polić, B. (2018). Virus-Induced Interferon-gamma Causes Insulin Resistance in Skeletal Muscle and Derails Glycemic Control in Obesity. *Immunity* 49, 164–177.e6.
228. Meisel, J.S., Hannigan, G.D., Tyldsley, A.S., SanMiguel, A.J., Hodkinson, B.P., Zheng, Q., and Grice, E.A. (2016). Skin Microbiome Surveys Are Strongly Influenced by Experimental Design. *J. Invest. Dermatol.* 136, 947–956.
229. He, Y., Wu, W., Zheng, H.M., Li, P., McDonald, D., Sheng, H.F., Chen, M.X., Chen, Z.H., Ji, G.Y., Zheng, Z.D., et al. (2018). Regional variation limits applications of healthy gut microbiome reference ranges and disease models. *Nat. Med.* 24, 1532–1535.
230. Gaulke, C.A., and Sharpston, T.J. (2018). The influence of ethnicity and geography on human gut microbiome composition. *Nat. Med.* 24, 1495–1496.
231. Rast, P., and Hofer, S.M. (2014). Longitudinal design considerations to optimize power to detect variances and covariances among rates of change: simulation results based on actual longitudinal studies. *Psychol. Methods* 19, 133–154.
232. Taris, T.W., and Kompier, M.A. (2006). Games researchers play—extreme-groups analysis and mediation analysis in longitudinal occupational health research. *Scand. J. Work Environ. Health* 32, 463–472.
233. Amrhein, V., and Greenland, S. (2018). Remove, rather than redefine, statistical significance. *Nat. Hum. Behav.* 2, 4.
234. Cady, N.C., Stelick, S., and Batt, C.A. (2003). Nucleic acid purification using microfabricated silicon structures. *Biosens. Bioelectron.* 19, 59–66.
235. Wasserstein, R.L., and Lazar, N.A. (2016). The ASA Statement on p-Values: Context, Process, and Purpose (Taylor & Francis).
236. Gruber, S., and Tchetgen Tchetgen, E. (2016). Limitations of empirical calibration of p-values using observational data. *Stat. Med.* 35, 3869–3882.
237. Benjamin, D.J., Berger, J.O., Johannesson, M., Nosek, B.A., Wagenmakers, E.J., Berk, R., Bollen, K.A., Brembs, B., Brown, L., Camerer, C., et al. (2018). Redefine statistical significance. *Nat. Hum. Behav.* 2, 6–10.
238. McShane, B.B., Gal, D., Gelman, A., Robert, C., and Tackett, J.L. (2019). Abandon statistical significance. *Am. Stat.* 73, 235–245.
239. Caporaso, J.G., Lauber, C.L., Walters, W.A., Berg-Lyons, D., Lozupone, C.A., Turnbaugh, P.J., Fierer, N., and Knight, R. (2011). Global patterns of 16S rRNA diversity at a depth of millions of sequences per sample. *Proc. Natl. Acad. Sci. USA* 108, 4516–4522.
240. Callahan, B.J., McMurdie, P.J., Rosen, M.J., Han, A.W., Johnson, A.J., and Holmes, S.P. (2016). DADA2: High-resolution sample inference from Illumina amplicon data. *Nat. Methods* 13, 581–583.

241. McMurdie, P.J., and Holmes, S. (2013). phyloseq: an R package for reproducible interactive analysis and graphics of microbiome census data. *PLoS One* 8, e61217.
242. Friedman, J., and Alm, E.J. (2012). Inferring correlation networks from genomic survey data. *PLoS Comput. Biol.* 8, e1002687.
243. Hummel, W., and Kula, M.-R. (1989). Simple method for small-scale disruption of bacteria and yeasts. *J. Microbiol. Methods* 9, 201–209.
244. Caporaso, J.G., Lauber, C.L., Walters, W.A., Berg-Lyons, D., Huntley, J., Fierer, N., Owens, S.M., Betley, J., Fraser, L., Bauer, M., et al. (2012). Ultra-high-throughput microbial community analysis on the Illumina HiSeq and MiSeq platforms. *ISME J.* 6, 1621–1624.
245. Minalla, A., Dubrow, R.S., and Bousse, L.J. (2001). Feasibility of High-Resolution Oligonucleotide Separation on a Microchip. *Proc. SPIE* 4560, Microfluidics and BioMEMS 1234.
246. Almonacid, D.E., Kraal, L., Ossandon, F.J., Budovskaya, Y.V., Cardenas, J.P., Bik, E.M., Goddard, A.D., Richman, J., and Apte, Z.S. (2017). 16S rRNA gene sequencing and healthy reference ranges for 28 clinically relevant microbial taxa from the human gut microbiome. *PLoS One* 12, e0176555.
247. Cole, J.R., Wang, Q., Fish, J.A., Chai, B., McGarrell, D.M., Sun, Y., Brown, C.T., Porras-Alfaro, A., Kuske, C.R., and Tiedje, J.M. (2014). Ribosomal Database Project: data and tools for high throughput rRNA analysis. *Nucleic Acids Res.* 42, D633–D642.
248. Kuczynski, J., Liu, Z., Lozupone, C., McDonald, D., Fierer, N., and Knight, R. (2010). Microbial community resemblance methods differ in their ability to detect biologically relevant patterns. *Nat. Methods* 7, 813–819.
249. Contrepois, K., Wu, S., Moneghetti, K.J., Hornburg, D., Ahadi, S., Tsai, M.S., Metwally, A.A., Wei, E., Lee-McMullen, B., Quijada, J.V., et al. (2020). Molecular Choreography of Acute Exercise. *Cell* 181, 1112–1130.e16.
250. Contrepois, K., Mahmoudi, S., Ubhi, B.K., Papsdorf, K., Hornburg, D., Brunet, A., and Snyder, M. (2018). Cross-Platform Comparison of Untargeted and Targeted Lipidomics Approaches on Aging Mouse Plasma. *Sci. Rep.* 8, 17747.
251. Hornburg, D., Wu, S., Moqri, M., Zhou, X., Contrepois, K., Bararpour, N., Traber, G.M., Su, B., Metwally, A.A., Avina, M., et al. (2023). Dynamic lipidome alterations associated with human health, disease and ageing. *Nat. Metab.* 5, 1578–1594.
252. Contrepois, K., Jiang, L., and Snyder, M. (2015). Optimized Analytical Procedures for the Untargeted Metabolomic Profiling of Human Urine and Plasma by Combining Hydrophilic Interaction (HILIC) and Reverse-Phase Liquid Chromatography (RPLC)-Mass Spectrometry. *Mol. Cell. Proteomics* 14, 1684–1695.
253. Röst, H.L., Schmitt, U., Aebersold, R., and Malmström, L. (2014). pyOpenMS: a Python-based interface to the OpenMS mass-spectrometry algorithm library. *Proteomics* 14, 74–77.
254. Röst, H.L., Liu, Y., D'Agostino, G., Zanella, M., Navarro, P., Rosenberger, G., Collins, B.C., Gillet, L., Testa, G., Malmström, L., et al. (2016). TRIC: an automated alignment strategy for reproducible protein quantification in targeted proteomics. *Nat. Methods* 13, 777–783.
255. Jiang, C., Zhang, X., Gao, P., Chen, Q., and Snyder, M. (2021). Decoding personal biotic and abiotic airborne exposome. *Nat. Protoc.* 16, 1129–1151.
256. Contreras, P.H., Salgado, A.M., Bernal, Y.A., and Vigil, P. (2019). A simple and improved predictor of insulin resistance extracted from the oral glucose tolerance test: The I0^G60. *J. Endocr. Soc.* 3, 1154–1166.
257. Kulesa, A., Krzywinski, M., Blainey, P., and Altman, N. (2015). Sampling distributions and the bootstrap. *Nat. Methods* 12, 477–478.
258. Shade, A., and Handelsman, J. (2012). Beyond the Venn diagram: the hunt for a core microbiome. *Environ. Microbiol.* 14, 4–12.
259. Risely, A. (2020). Applying the core microbiome to understand host-microbe systems. *J. Anim. Ecol.* 89, 1549–1558.
260. Salonen, A., Salojärvi, J., Lahti, L., and de Vos, W.M. (2012). The adult intestinal core microbiota is determined by analysis depth and health status. *Clin. Microbiol. Infect.* 18, 16–20.
261. Bates, D., Mächler, M., Bolker, B., and Walker, S. (2015). Fitting Linear Mixed-Effects Models Using lme4. *J. Stat. Software* 67, 1–48.
262. Nelson, L.S. (1998). The Anderson-Darling Test for Normality. *J. Qual. Technol.* 30, 298–299.
263. Johnson, S.G. (2011). The NLOpt nonlinear-optimization package. <http://ab-initio.mit.edu/nlopt>.
264. Zeileis, A., and Hothorn, T. (2002). Diagnostic checking in regression relationships. <https://cran.r-project.org/web/packages/lmtest/vignettes/lmtest-intro.pdf>.
265. Satterthwaite, F.E. (1946). An approximate distribution of estimates of variance components. *Biometrics* 2, 110–114.
266. Bürkner, P.-C. (2017). brms: An R package for Bayesian multilevel models using Stan. *J. Stat. Software* 80, 1–28.
267. Bürkner, P.-C. (2017). Advanced Bayesian Multilevel Modeling with the R package brms. Preprint at arXiv 17234. <https://doi.org/10.48550/arXiv.1705.11123>.
268. Bürkner, P.-C. (2021). Bayesian Item Response Modeling in R with brms and Stan. *J. Stat. Software* 100, 1–54.
269. Hoffman, M.D., and Gelman, A. (2014). The No-U-turn sampler: adaptively setting path lengths in Hamiltonian Monte Carlo. *J. Mach. Learn. Res.* 15, 1593–1623.
270. Altman, D.G., and Bland, J.M. (2011). How to obtain the P value from a confidence interval. *BMJ* 343, d2304.
271. Fang, H., Huang, C., Zhao, H., and Deng, M. (2015). CCLasso: correlation inference for compositional data through Lasso. *Bioinformatics* 31, 3172–3180.
272. Hughes, D.A., Bacigalupe, R., Wang, J., Rühlemann, M.C., Tito, R.Y., Falony, G., Joossens, M., Vieira-Silva, S., Henckaerts, L., Rymenans, L., et al. (2020). Genome-wide associations of human gut microbiome variation and implications for causal inference analyses. *Nat. Microbiol.* 5, 1079–1087.
273. Koh, A., and Bäckhed, F. (2020). From Association to Causality: the Role of the Gut Microbiota and Its Functional Products on Host Metabolism. *Mol. Cell* 78, 584–596.
274. Fu, W. (2019). Statistical Issues in Microbiome Data Analysis: Batch Effects and Multi-omics Analysis. <http://hdl.handle.net/1773/44069>.
275. Schaum, N., Lehallier, B., Hahn, O., Pálócs, R., Hosseinzadeh, S., Lee, S.E., Sit, R., Lee, D.P., Losada, P.M., Zardeneta, M.E., et al. (2020). Ageing hallmarks exhibit organ-specific temporal signatures. *Nature* 583, 596–602.
276. Boedigheimer, M.J., Wolfinger, R.D., Bass, M.B., Bushel, P.R., Chou, J.W., Cooper, M., Corton, J.C., Fostel, J., Hester, S., and Lee, J.S. (2008). Sources of variation in baseline gene expression levels from toxicogenomics study control animals across multiple laboratories. *BMC Genomics* 9, 1–16.
277. Poore, G.D., Kopylova, E., Zhu, Q., Carpenter, C., Fraraccio, S., Wandro, S., Kosciok, T., Janssen, S., Metcalf, J., and Song, S.J. (2020). Microbiome analyses of blood and tissues suggest cancer diagnostic approach. *Nature* 579, 567–574.
278. Wood, S.N. (2004). Stable and efficient multiple smoothing parameter estimation for generalized additive models. *J. Am. Stat. Assoc.* 99, 673–686.

STAR★METHODS

KEY RESOURCES TABLE

REAGENT or RESOURCE	SOURCE	IDENTIFIER
Biological samples		
EDTA-plasma and PBMCs prepared from intravenous whole blood collection	this manuscript	N/A
Stool Sample	this manuscript	N/A
Skin Swaps	this manuscript	N/A
Oral Swaps	this manuscript	N/A
Nasal Swaps	this manuscript	N/A
Chemicals, peptides, and recombinant proteins		
MO BIO's PowerSoil DNA Isolation Kit	Qiagen	47014
AllPrep DNA/RNA/Protein kit	Qiagen	80004
Critical commercial assays		
Insulin-Suppression Test	Stanford's Clinical and Translational Research Unit	https://med.stanford.edu/ctr/services.html#laboratory-services
Luminex Multiplex Assays	Stanford Human Immune Monitoring Center	https://iti.stanford.edu/himc/immunoassays.html
Microbial 16S rRNA V4 sequencing	uBiome	Caporaso et al. ²³⁹
Clinical Lab Test	Stanford's Clinical and Translational Research Unit	https://stanfordlab.com/test-directory.html
Deposited data		
Raw 16S rRNA V4 sequencing data, skin and oral	this manuscript	https://hmpdacc.org
Raw 16S rRNA V1-3 sequencing data, stool and nasal	Zhou et al. ⁷⁰	https://hmpdacc.org
Oligonucleotides		
27F: 5'-AGAGTTTGATCCTGGCTCAG-3'	this manuscript	N/A
534R: 5'-ATTACCGCGGCTGCTGG-3'	this manuscript	N/A
515F: 5'-GTGCCAGCMGCCGCGGTAA-3'	uBiome	Caporaso et al. ²³⁹
806R: 5'-GGACTACHVGGGTWTC TAAT-3'	uBiome	Caporaso et al. ²³⁹
Software and algorithms		
BCL2FASTQ2	Illumina	https://support.illumina.com/sequencing/sequencing_software/bcl2fastq-conversion-software.html
DADA2	GitHub ²⁴⁰	https://benjjneb.github.io/dada2/
Phyloseq	Bioconductor ²⁴¹	https://bioconductor.org/packages/release/bioc/html/phyloseq.html
SPARCC	GitHub ²⁴²	https://rdrr.io/github/siskac/discordant/src/R/SparCC.R
igraph	Bioconductor	https://igraph.org/
Other		
Human Microbiome Project – Core Microbiome Sampling Protocol A	HMP Protocol ⁷⁰	# 07-001, v12.0

RESOURCE AVAILABILITY

Lead contact

Further information and requests for resources and reagents should be directed to and will be fulfilled by the lead contact, Michael P. Snyder (mpsynder@stanford.edu).

Materials availability

This study did not generate new unique reagents.

Data and code availability

The microbiome data are available at <https://hmpdacc.org>. Other omics data can be accessed through Stanford iPOP website at <https://med.stanford.edu/ipop.html>.

The microbiome data specific to this study can be accessed at GitHub Repository (<https://github.com/xzhou7/iHMP>). The meta-data corresponding to these data files can be found at Stanford Data Repository (<http://hmp2-data.stanford.edu/script.php?table=subject>).

Any additional information required to reanalyze the data reported in this paper is available from the [lead contact](#) upon request.

EXPERIMENTAL MODEL AND SUBJECT DETAILS

Human Cohort

Our study was conducted as part of the integrated Human Microbiome Project of the National Institutes of Health (NIH). This human study was approved by Stanford University's Institutional Review Boards (#23602), ensuring ethical compliance and participant safety. Informed consent was obtained from all participants, who were either at risk for type 2 diabetes or voluntarily interested in diabetes-related research.

Eligible participants were either at risk for type 2 diabetes or voluntarily interested in diabetes-related research. Exclusion criteria encompassed hypertriglyceridemia > 4.0 mg/ml⁻¹, uncontrolled hypertension, uncontrolled psychiatric disease, previous bariatric surgery, pregnancy or lactation, eating disorders (i.e., binge eating disorder, anorexia nervosa, or bulimia nervosa), alcohol use disorder, or failure to provide five consecutive samples from at least one body site (stool, skin, nasal, or oral). Consequently, data from 86 participants met the criteria for inclusion in this analysis.

Regarding the allocation of subjects to experimental groups, participants were not divided into separate experimental groups per se, but rather contributed samples for comprehensive microbiome analysis. This approach was designed to capture a broad spectrum of microbiome data across different body sites.

In our analysis, we considered the impact of various factors, including biological age, gender, self-reported ethnicity on the study's outcomes. These factors were included in our linear mixed model (LMM) for intra class correlations. Members within the same household were compared for the family score computation.

METHOD DETAILS

Microbiome sample collection and sequencing

Stool samples were self-collected by participants and other HMP samples were collected by study coordinators following iPOP study standard operating procedures (SOP), as adapted from HMP_SOP corresponding sections (HMP_MOP_Version12_0_072910).⁷⁰ Briefly, retroauricular areas were rubbed with pre-moistened swabs under pressure for skin sampling, anterior nares for nasal sampling, and rear of the oropharynx for oral sampling. Samples are stored at -80 C immediately after arrival. Stool and nasal samples were further processed and sequenced in-house at the Jackson Laboratory for Genomic Medicine (JAX-GM, Farmington, CT, USA) and detailed methods are described previously,⁷⁰ while oral and skin samples were sent to uBiome (uBiome, San Francisco, CA, USA) for further processing.

After 30 minutes of beads-beating lysis, skin and oral samples were processed using a silica-guanidinium thiocyanate-based nucleic acid isolation protocol^{234,243,244} on a liquid-handling robot. The 16S rRNA variable region V4 was amplified by 35 cycles of PCR using the primer 515F (5'-GTGCCAGCMGCCGCGGTAA-3') and 806R (5'-GGACTACHVGGGTWTC TAAT-3').²³⁹ The DNA from each sample was barcoded and combined to create a sequencing library. The sequencing library was then purified using columns and microfluidic DNA fractionation²⁴⁵ to reduce unwanted DNA fragments. Bio-Rad MyiQ was used to quantify the DNA concentration of the library using the Kapa iCycler qPCR kit (Bio-Rad Laboratories, Hercules, CA, USA). Sequencing was performed on the Illumina NextSeq 500 Platform (Illumina, San Diego, CA, USA) via 2 * 150 bp paired-end sequencing protocol.²⁴⁶

Raw sequencing data from the stool samples and nasal samples are acquired from our previous publication.⁷⁰ Briefly, 16S rRNA gene from V1~V3 hyper-variable region was sequenced with primer pair of 27F (5'-AGAGTTTGATCCTGGCTCAG-3') and 534R (5'-ATTACCGCGGCTGCTGG-3') and being barcoded and sequenced on the Illumina MiSeq sequencing platform through a V3 2 × 300 sequencing protocol. The same cutoff used in skin and oral sequencing data was applied to stool and nasal sequencing data in demultiplexing. After demultiplexing, reads with Q-scores less than 35 and ambiguous bases (Ns) are trimmed for additional analysis.

Microbiome data processing

Demultiplexed sequenced samples were saved as FASTQ files using BCL2FASTQ software (Version 2.20, Illumina, CA, USA). Sequences with barcode mismatches, primer mismatches exceeding one, or Q-scores below 30 were excluded. Due to low overlap between forward and reverse reads according to FLASH (Version 1.2.11), only forward reads were selected for further processing.

Microbiome sequencing data from four body sites were combined and processed using the DADA2 R package (version 1.16).²⁴⁰ Sequences were filtered to remove ambiguous bases (maxN=0) and those with more than two expected errors (maxEE=2). After

filtering, inter-sample composition analysis was performed based on the learned error rate. An amplicon sequence variant (ASV) table was constructed, and chimeras were removed using the DADA2 workflow consensus method. Reads passing all filters were aligned against a trained database of target 16S rRNA gene sequences and taxonomic annotations derived from Version 18 of The Ribosomal Database Project (RDP)²⁴⁷ Taxonomy release (Aug 14, 2020). Relative ASV abundance was determined by dividing the count associated with that taxon by the total number of filtered reads. Samples with depths below 1,000 reads were removed due to insufficient sequencing depths²⁴⁸ following the HMP consortium standard.^{15,70} The Local Outlier Factor (LOF) of each point was calculated on a sequencing depth to richness (observed ASV) plot, and samples with a LOF greater than 3 (n=7) were removed due to an abnormal richness-sequencing depth relationship. The average sample sequencing depth after quality control was 23,554 for stool microbiome, 74,515 for skin microbiome, 132,912 for oral microbiome, and 24,899 for nasal microbiome. Batch effects were estimated using PERMANOVA analysis when both batch and subject ID were included, with results showing that the total variance explained by the 23 batches was 2% for stool, 3% for nasal, 0.6% for oral, and 3.6% for skin samples. The batch effects were considered small, and no correction for batch effects was applied in the analysis.

Lipidomics analyses

Lipid extraction and data generation were performed as previously described.^{249–251} Briefly, complex lipids were extracted from 40 μ L of EDTA-plasma using a mixture of methyl tertiary-butyl ether, methanol, and water, followed by biphasic separation. Lipids were then analyzed using the Lipidizer platform, which consists of a DMS device (SelexION Technology, Framingham, MA, USA) and a QTRAP 5500 (Sciex). Lipids were quantified using a mixture of 58 labeled internal standards provided with the platform (cat# 5040156, Sciex, Redwood City, CA, USA), and lipid abundances were reported in nmol/g.

To address the high collinearity of the lipidomic data, a customized clustering method was designed. Specifically, the lipidomics data were divided into six clusters using Fuzzy c-means clustering (R package “Mfuzz” (version 3.15)). For the lipids within each cluster, correlations were computed, and lipids with high correlative relationships (Spearman correlation > 0.8 and BH-adjusted p-values < 0.05) were grouped into the same module. Community analysis (“fastgreedy.community” function from R package “igraph” (v1.3.5)) was employed to detect the modules. For lipids not assigned to any of the modules, their original lipid species annotations were used for downstream analysis (Table S5A).

Metabolomics Analyses

Untargeted metabolic profiling was performed using a broad-spectrum LC-MS platform using a combination of reverse-phase liquid chromatography (RPLC) and hydrophilic interaction liquid chromatography (HILIC) separations and high-resolution MS.^{70,252} Briefly, plasma metabolites were extracted following solvent precipitation using a mixture of ice-cold acetone, acetonitrile, and methanol (1:1:1, v/v). Hydrophilic metabolites were separated on a ZIC-HILIC (2.1 \times 100 mm, 3.5 μ m, 200 \AA ; Merck Millipore) while hydrophobic metabolites were separated on a Zorbax SBAq columns (2.1 \times 50 mm, 1.7 μ m, 100 \AA ; Agilent Technologies). Data was acquired on a Thermo Q Exactive plus mass spectrometer for HILIC and a Thermo Q Exactive mass spectrometer for RPLC. Raw data were processed using Progenesis QI (v2.3, Nonlinear Dynamics, Waters) and metabolites were formally identified by matching fragmentation spectra and retention time to analytical-grade standards or matching experimental MS/MS to fragmentation spectra in publicly available databases. A total of 726 annotated metabolites were retained for downstream analysis.

Proteomics analyses

Plasma proteins were characterized using a TripleTOF 6600 system (Sciex) via liquid chromatography-mass spectrometry (LC-MS) with SWATH acquisition, following the methodology outlined in a previous study.⁷⁰ In every injection, 8- μ g of tryptic peptides, derived from undepleted plasma, were loaded onto a ChromXP C18 column (0.3 \times 150 mm, 3 μ m, 120 \AA , Sciex). The separation of peptides was achieved through a 43-minute gradient ranging from 4% to 32% B. High sensitivity MS/MS mode was utilized to construct variable Q1 window SWATH Acquisition methods (100 windows) with Analyst TF Software (v1.7). Scoring of peak groups was performed with PyProphet (v2.0.1)²⁵³ and alignment of peak groups with TRIC,²⁵⁴ each adhering to stringent confidence thresholds (1% FDR at peptide level; 10% FDR at protein level). The abundance of proteins was calculated as the cumulative sum of the three most abundant peptides.

Luminex multiplex assays for targeted cytokine, chemokine, and growth factors

The evaluation of circulating cytokines, chemokines, and growth factors was undertaken employing established procedures from the Stanford Human Immune Monitoring Center (HIMC). Specifically, EDTA-plasma was scrutinized using a Human 62-plex Luminex multiplex assay, consisting of conjugated antibodies (Affymetrix, Santa Clara, California). The raw data obtained from the assay were normalized against the median fluorescence intensity (MFI) value. Subsequently, variance stabilizing transformation (VST) was applied to the data to eradicate the batch effect, adhering to our previously outlined methodology.¹⁴⁵ Measurements featuring background noise (CHEX) exceeding five standard deviations from the mean (mean \pm 5 \times SD) were omitted from the data.

Exposome and associated environmental analyses

As previously outlined,^{90,255} the process of data collection for the exposome and associated environmental elements proceeded accordingly. The chemical exposome was sampled using the RTI MicroPEM V3.2 personal exposure monitor (RTI International, Research Triangle Park, NC, USA) for two participants. The MicroPEM, an active air sampling apparatus, operates by circulating

air at a rate of 0.5 L/min. It was modified to house a customized cartridge containing 200 mg of zeolite adsorbent beads (Sigma 2-0304, Sigma-Aldrich Corp., St. Louis, MO USA) positioned at the airflow's termination to gather both hydrophobic and hydrophilic compounds. Each sampling session spanned approximately five days. Post-session, the cartridge was detached and preserved at -80 °C until subsequent processing. Chemical extraction involved the resuspension of zeolite beads in a sterile Eppendorf LoBind tube filled with 1 mL of Mass Spec grade methanol. Following a 20-minute incubation period at room temperature, the samples were subjected to a 20-minute centrifugation process at 22,000 g, also at room temperature. The samples were then analyzed using a Waters UPLC-coupled Exactive Orbitrap Mass Spectrometer (Thermo, Waltham, MA, USA), yielding a collection of 158 exposome chemicals. Environmental data, on the other hand, were sourced from several origins. Parameters such as temperature, humidity, and sampling flow rate were directly recorded by the MicroPEM. GPS coordinates of the participants provided geographical data. Additional meteorological and demographic information was obtained from public data repositories including the Climate Data Online (CDO), the US Census Bureau, and local weather stations. This culminated in the collection of 10 environmental feature data points.

Dietary analyses

A total of 25 food items were included in a questionnaire that was completed voluntarily by participants during their routine visit in the study, using a diet questionnaire hosted on <https://www.projectredcap.org/> from our previous report.¹⁴⁵ The frequency of consuming each food item was scored in downstream analysis. For breads, biscuits, cakes, pies and pastries, we score the frequency from 0~4, with the associated frequency per day: 0) less than 1, 1)1 per day, 2)2~3 per day, 3)4~5 per day, 4)6 or more. For other foods we ask the participants to state the frequency from 6+ times per day to less than once per month.

Insulin-suppression test

A subset of eligible consenting participants (N=58) underwent an Insulin-Suppression Test (IST), as a measure of insulin-mediated glucose uptake, to evaluate the insulin sensitivity status. Following a 12-hour overnight fast, participants were administered an infusion comprising 0.27 ug/m² min of octreotide, 25m U/m² min of insulin, and 240 mg/m² min of glucose over a three-hour period during their visit to Stanford's Clinical and Translational Research Unit (CTRU). Blood samples were procured at ten-minute intervals during the final half-hour of the infusion, resulting in a total of four blood draws. These samples were analyzed to determine plasma glucose and insulin levels. The mean value of the four steady-state plasma glucose (SSPG) and insulin concentrations were subsequently calculated. Participants were then categorized based on their SSPG values²⁵⁶: those with SSPG < 150 mg/dl were classified as insulin sensitive (IS) (n=28), while those with SSPG ≥ 150 mg/dl were classified as insulin resistant (IR) (n =30). Participants who were unable to provide measurements due to personal or medical circumstances were allocated to an indeterminate group (Unknown) (n= 28).

Clinical lab test

Clinical lab tests were performed at the Stanford Clinical Lab following its guideline of blood and urine collection and submission (<https://stanfordlab.com/test-directory.html>). The test includes a metabolic panel, complete blood count panel, glucose, HbA1C, insulin measurements, hsCRP, IgM, lipid panel, kidney panel, liver panel. Detailed measurements and annotations are provided as a supplementary table (Table S6A).

QUANTIFICATION AND STATISTICAL ANALYSIS

UMAP for microbiome distribution

The distribution of the microbiome was visualized using Uniform Manifold Approximation and Projection (UMAP), facilitated by the R package "Seurat (Version 4.0)". Prior to the application of UMAP, the count data were first normalized to relative abundance and scaled to represent one million reads per sample. A total of 1524 variable features were identified and encapsulated within a Seurat object. From this point, a distance matrix was produced through the utilization of the R package "Vegan (Version 2.6-2)", employing Bray Curtis dissimilarity. This distance matrix was subsequently transformed via Principal Coordinate Analysis (PCoA). The first ten dimensions from the PCoA (out of a total of 1094 generated) were used to determine neighboring relationships. The UMAP projection was then calculated, with default settings employed. This projection was made possible by invoking Python's UMAP via reticulate. The final UMAP results were visualized using the first two dimensions.

Intraclass correlation

Intraclass correlation Coefficient (ICC) was calculated from Linear Mixed Models, in which we modeled random intercepts but a fixed slope, allowing different personal levels between individuals.⁷⁰ We first linearly transformed each analyte (when applicable) and standardized the total variation to 1 before applying 'lmer' function from R package "lme4 (V1.1-30)", with the formula as:

$$Exp \sim 1 + Days + (1|SubjectID)$$

Where *Exp* was the linearly transformed and standardized values of each analyte, *Days* was the length of time individuals participated in the study, *SubjectID* was the subject ID associated with each participant.

We then used ICC as the proportion of total variation explained by subject structure in the cohort by $V_{\text{subjectID}}/V_{\text{total}}$, in which V was the variance from the corresponding component extracted by Var_{Corr} and V_{total} was 1.

Permutation test on Bray Curtis Distance Comparison

The Bray-Curtis (BC) distance was used to quantify the degree of similarity between two microbiome samples, with the ASV serving as the unit for calculating dissimilarity for the complete microbiome sample or for specific taxa. Similarity metrics were calculated pairwise for both intra-individual and inter-individual comparisons. A permutation test was employed to estimate the null distribution while accounting for the varying sample sizes of each participant. The null hypothesis being tested was that there is no difference between intra-individual and inter-individual distances.

For each microbial genus, a test statistic was calculated as the mean difference in BC distances between intra-individual and inter-individual comparisons. To estimate the null distribution, all sample labels were randomly permuted, and the BC distances were computed pairwise. This process was repeated 10,000 times, generating a null distribution of test statistics.

P-values were then calculated by determining the proportion of permuted test statistics that were at least as extreme as the observed test statistic. In the case of multiple comparisons, such as for different microbial genera, p-values were adjusted using the BH procedure to control the false discovery rate. Statistical significance was determined using a threshold of BH adjusted p-value < 0.1.

Degree of microbial individuality

Degree of Microbial Individuality (DMI) was measured as the mathematical difference between a given genus regarding their populational median of the inter-individual BC distance and the median of the intra-individual BC distance. To assess the robustness and variability of the DMI estimates, we employed a bootstrap resampling technique.²⁵⁷

First, we summarized the between-sample distance of genera with longitudinal prevalence greater than 10% at a given body site. The distance of sample pairs was then allocated into inter-individual or intra-individual groups. For each genus, we resampled the data with replacement and computed the DMI using the following formula:

$$DMI_i = BC_{\text{inter-individual}} - BC_{\text{intra-individual}}$$

This resampling process was repeated multiple times to obtain a distribution of DMI estimates, which enabled us to assess the variability and robustness of our results.

By employing the bootstrap resampling technique, we aimed to gain insights into the reliability of our DMI calculations and understand how sensitive they were to potential variations in the data. This approach provided a more comprehensive understanding of the degree of microbial individuality across various body sites and taxa. To ensure the accuracy of our results, we considered a DMI to be reliable only if that DMI's standard deviation (SD) of the bootstrapped distribution is less than 15 times of the mean DMI. This criterion helped to filter out any DMI estimates that might be influenced by high variability or uncertainty in the data. Detail of the bootstrap result was included in our supplementary materials (Table S2C), where we used column "confidence" to distinguish DMI values with high or low reliability. The total number of genera reported per region after bootstrapping included: 105 for stool, 35 for skin, 63 for oral, and 33 for nasal samples.

To quantify the cumulative DMI for each individual, the DMI score was multiplied by the average relative abundance of each genus for a given individual. This generated a weighted DMI (abundance_dmi) that represented the product of the DMI score and the genus's relative abundance. The total DMI for each individual was computed by summing these weighted DMI values across all genera. This approach offered a comprehensive measure of the overall DMI per individual, accounting for the contribution of each genus weighted by its relative abundance in the individual's microbiome.

Family score

To assess the impact of a shared living environment on microbiome variability, we introduced a metric called the Family Score (FS). The FS represents the relative influence of a shared environment on the inter-individual dissimilarity of a given genus within cohabitating pairs. We began by excluding genera with a longitudinal prevalence of less than 10%, leaving 141 for stool, 119 for skin, 41 for oral, and 33 for nasal samples. For each remaining genus, we computed the "within-family" inter-individual Bray-Curtis (BC) distance between cohabitating pairs. We also calculated the median inter-individual BC distance (BC inter-individual) and intra-individual BC distance (BC intra-individual). Using these values, we computed the FS for a given genus 'i' with the following formula:

$$\text{Family Score}_i = (BC_{\text{inter-individual}} - BC_{\text{intra-family}}) / (BC_{\text{inter-individual}} - BC_{\text{intra-individual}})$$

This formula normalizes the FS to a scale that allows for comparisons across families and non-families. An FS of 0 indicates that the shared living environment has no impact on inter-individual dissimilarity, while an FS of 1 suggests that living in the same environment causes inter-individual dissimilarity to resemble intra-individual dissimilarity. We truncated the FS at 0 and 1 to maintain consistency in the comparison scale. Any FS values greater than or equal to 1 were assigned a value of 1, and values less than or equal to 0 were assigned a value of 0.

Classification of the microbiome genera by their longitudinal prevalence

The microbiome genera were categorized as the core microbiome, opportunistic microbiome, and middle group based on their longitudinal prevalence.^{258–260} Calculation of prevalence was based on the presence or absence of reads from each sample. For each

sample, the relative abundance of each genus was first transformed to 1 if it was greater than 0; then, the proportion of 1 for each genus in each participant was determined as the longitudinal prevalence. Then the genera were assigned to a group based on their longitudinal prevalence: core microbiome: longitudinal prevalence > 80%; middle group: 20% ≤ longitudinal prevalence ≤ 80%; opportunistic microbiome: longitudinal prevalence < 20%.

Body site-specific longitudinal model for Bray-Curtis distance

To estimate the effect of body site on the change in BC distance over time, we used a linear mixed effects regression with the BC distance as the response variable implemented in the “lme4” package in R.²⁶¹ The BC distance of all pairwise samples was transformed to a more normally distributed dataset. The transformation method used was the log-log transformation, which has been widely used in survival analysis studies. Specifically, the transformation was performed by applying the formula:

$$\text{transformed_dist} = \log_{10}(-\log_{10}(1-\text{dist}))$$

A total of eight different transformations were evaluated (variations of logarithmic, square root, arcsine, and ratio transformations of the original distance) to identify the most suitable transformation for our analysis. To assess the normality of the transformed distances, an Anderson-Darling test was performed, and the best method was selected by Anderson-Darling’s statistics A.²⁶²

Fixed effects included an interaction between the body site and time, and with a random intercept for each individual. Time was normalized to the days from the first sample for each individual. The model was optimized using the “nloptwrap” method²⁶³ and nested models were compared by likelihood ratio test using the “lmerTest” package in R.²⁶⁴ Differences in the slopes of the body sites over time were assessed by F-test with Satterthwaites’s degrees of freedom.²⁶⁵ For the comparisons between body sites, the model was constructed as:

$$\text{dist} \sim -1 + \text{diffdays} * \text{dataset} + (1 | \text{subject_id})$$

For the comparison between IR and IS participants, the model was constructed as:

$$\text{dist} \sim -1 + \text{IRIS} * \text{diffdays} + (1 | \text{subject_id}) + (1 + \text{IRIS} | \text{subject_id})$$

Where *dist* was the pairwise BC distance, *diffdays* was the date interval between two samples, *subject_id* was the subject ID associated with each participant, and *IRIS* was the insulin sensitivity status of each participant.

Bayesian mixed-effects model for microbial taxa and cytokine interactions

We utilized a Bayesian negative-binomial longitudinal mixed-effects model to analyze the interactions between microbial taxa and cytokines. This model choice addresses several key characteristics of our data: the compositional nature of microbiome data, the presence of zero-inflation and high skewness in cytokine measurements, and the repeated measurements of both cytokine and microbiome data in our study cohort (n=62 with longitudinal, date-matching measurements). The model’s capacity to handle the highly skewed cytokine data was a critical factor in its selection, especially given the dramatic range of cytokine surges observed in our dataset, ranging from a 10.8-fold increase for MIP1B to as much as a 618-fold increase for LEPTIN. Each genus’s reads count was modeled as a sparse-matrix response variable, with a plasma cytokine level MFI quantity and time as fixed effects and a random intercept for each individual, following the formula:

$$M_i = X_i \beta + Z_i b_i + \epsilon_i$$

Where *M_i* is a vector of the genus-level microbe relative abundances for each participant *i*, *X_i* is the design matrix for the fixed effects, β . Each row of matrix *X_i* contains the terms (1) time (days post-study start), *D_i*, and (2) cytokine measurements, *Y_i*, from 1 to *n*. *Z_i* is the random effects design vector of 1’s denoting a random intercept, *b_i* is a scalar for each participant, and ϵ_i is a zero-centered error term.

Posterior sampling was performed using four chains, 5,000 iterations per sample, and a 1,000-iteration burn-in of a No-U-Turn Sampler implemented in the “brms (Version 2.18.0)” package in R.^{266–269} The iteration plots and posterior predictive distributions were visually inspected for chain convergence. Microbe genera and cytokines above the limit of detection in less than 10% of the samples were excluded from the analysis. A microbe-cytokine association was considered significant if the 95% credible interval on the fit coefficient of the cytokine term did not include zero.

In our model, the beta represents the effect size. We estimated the variance explained by the model using the “bayes_R2” function from the brms package, and this information is included in the final table. While we provide p-values for each pair, as inferred from a method detailed previously,²⁷⁰ and the subsequent BH-adjusted p-values, it’s important to note that these are supplementary. In our Bayesian analysis, the determination of significance is based on the commonly practiced use of credible intervals derived from Markov Chain Monte Carlo (MCMC) sampling.

Correlation network analysis

Correlation network analysis was conducted to construct a network between the microbiome (from stool, skin, oral, and nasal samples) and internal multi-omics data (proteome, metabolome, and lipidome) from plasma, following a modified version of published methods.⁷⁰ Initially, time points with unmatched collection dates for each pair of microbiome and internal omics data were excluded. Subjects with fewer than five samples for a specific microbiome type were also removed from the corresponding correlation analysis.

The microbiome data, which included relative abundance or observed ASV richness at the genus level, was processed by retaining only genera detected in at least 10% of all samples. Centered log ratio (CLR) normalization was applied to address compositionality in microbiome data using the R package "compositions" (Version 2.0-4). Proteome, metabolome, and lipidome module data were \log_2 transformed.

To account for repeated sampling from the same subject, a linear mixed-effects model was utilized, incorporating subject ID as a random effect using the R package "lme4" (Version 1.1-30). Spearman correlations were then calculated, and p-values were adjusted using the Benjamini & Hochberg method. For correlation network construction, BH adjusted p-values < 0.2 were included. In the linear mixed model assessing longitudinal effects, the estimated correlation coefficient served as the measure of effect size (Figure S6B).

To gauge the robustness of the point estimation for the proportion of microbiome genera that are significantly correlated, we employed a bootstrapping approach. Specifically, we determined the percentage of significantly correlated genera by dividing the number of significantly correlated pairs by the total possible pairs. We bootstrapped this procedure 20 times to obtain mean and standard deviation values for the percentage of significantly correlated microbiome genera. These values were then used to compare the scale of interdependency of microbiome across different body sites. To ascertain if one body site exhibits a significantly greater interdependency compared to another, we employed the two-sided Wilcoxon rank-sum test. The significance of these comparisons was determined using p-values adjusted for multiple testing using the BH correction.

The estimation of inter-individual microbiome-wide correlation was conducted utilizing the SparCC method (R package *discordant*, Version 1.25.0), a methodology specifically tailored for compositional data.^{242,271} To prepare the microbiome relative abundance data for this analysis, the data were multiplied by 20000 and subsequently rounded, a process designed to convert proportions into data resembling counts. Following this, the SparCC method was employed to compute the correlation matrix. This matrix was then transformed into a long format data frame, with each row representing a pair of genera and their corresponding correlation coefficient. To assess the statistical significance of the observed correlations, a permutation test was implemented. For each pair of genera, the sample labels were randomly permuted, and the permuted SparCC correlation coefficient was calculated. We executed this procedure 10,000 times to produce a null distribution of SparCC correlation coefficients. Following this, we counted the instances where our observed correlation coefficient was encompassed within this null distribution. A finding was deemed "non-significant" if the correlation coefficient from any of the 10,000 permutations was more extreme than the coefficient from our original analysis, and subsequent raw p-value was computed based on the permutation results. Results with the BH adjusted p-value < 0.1 from this permutation was included in our final report.

The inter-omics correlation network was visualized using the R packages "ggraph" (Version 2.0.5), "igraph" (Version 1.3.2), and "tidygraph" (Version 1.2.1) under the "kk" layout.

Pathway enrichment for proteins correlated with the microbiome

The enrichment of pathways corresponding to proteins associated with the microbiome from four different body sites was achieved via the R package "clusterProfiler (Version 3.15)". The proteins in question served as input for pathway enrichment, specifically through Gene Ontology (GO) processes, enabling the identification of statistically significant pathways. The determination of these pathways was reliant on Fisher's exact test.

GO terms of interest were isolated based on their Benjamini-Hochberg adjusted p-values; terms with p-values below 0.05 were retained for ensuing analyses. For the GO terms that demonstrated significant enrichment, the R package "simplifyEnrichment" was employed. This package facilitated the calculation of similarities between each pair of GO terms. The construction of a network only incorporated edges that exhibited similarities exceeding 0.70.

In order to discern modules within the correlation network, community analysis was undertaken utilizing the R package "igraph (Version 1.3.4)". To encapsulate each module, only the GO term that presented with the smallest Benjamini-Hochberg adjusted p-value was preserved.

Mediation analysis

A mediation analysis was conducted to investigate the potential influence of microbiomes from stool, skin, oral, and nasal sources on phenotypes through internal multi-omics data, including proteome, metabolome, lipidome, and cytokine.^{56,272,273} Phenotype data were obtained via clinical laboratory tests of plasma samples. The associations between the microbiome and phenotype (Direct Effect), as well as internal omics data (Indirect Effect), were initially determined as outlined in the 'correlation network analysis' section. Only significant associations (BH adjusted p-values < 0.2) were considered for subsequent mediation analysis. The linear regression model from R package "mediation" was employed for the mediation analysis. Ultimately, pairs with significant Average Causal Mediation Effects (ACME, p-values < 0.05) were reported, representing the microbiome's impact on phenotype measurements through internal multi-omics.

To control the false discovery rate (FDR), a reverse mediation analysis was performed by exchanging the mediator with effects (i.e., the microbiome influencing internal omics data via phenotype), and pairs with significant ACME in reverse mediation (p-values < 0.05) were excluded from the final results. Comparisons between body sites and insulin sensitivity statuses were conducted for each dataset using the Fisher exact test. Initially, it was hypothesized that the true meditative effect of each mediated pathway (e.g., genus $i \sim$ cytokine $j \sim$ immune k) was considerably large ($n = 1 \times 10^8$). Subsequently, the presence of a significantly different meditative linkage between the designated comparison pairs was assessed.

Principal variance component analysis (PVCA)

To assess the variation in microbiome data based on individual and season, the principal variance component analysis (PVCA)²⁷⁴ was performed via R package "pvca (Version 3.15)". The PVCA is a combination of the principal component analysis and variance components analysis <https://www.niehs.nih.gov/research/resources/software/biostatistics/pvca/index.cfm>, which were originally employed to assess batch effects in microarray data²⁷⁵ and widely used for microbiome related variance decompositions.^{276,277} For microbiome samples in each body site, the season was determined by subtracting the date of collection from the first day of the year (from 1-365 days). Each sample's participant ID and season were then entered into the PVCA as variables. Then, the "ggtern (Version 3.3.5)" R package was used to visualize the data.

Deconvolute the environmental effect on the microbiome

Exposome and diet data analysis

To investigate the influence of exposome and diet data on the microbiome from different body sites, exposome data (chemical and environmental) were collected and processed as previously described.²⁵⁵ Diet data were collected and detailed in the methods section above. As an example, the analysis process for exposome chemical data is described below.

Microbiome samples with matching exposome chemical data within a 3-day period were selected for subsequent analysis ($N_{\text{Chemical}} = 8$, $N_{\text{Environmental}} = 32$ ($N_{\text{Participant1}} = 13$; $N_{\text{Participant2}} = 19$)). Microbiome data were normalized using the centered log ratio (CLR, "clr" function from R package "compositions"), and exposome data were \log_2 -transformed and auto-scaled.⁹² Principal component analysis (PCA) was performed on both microbiome and exposome data. Principal components (PCs) from the microbiome and exposome were further analyzed, with PCs accounting for over 80% of cumulative explained variation being included. A linear regression model was constructed using PCs of microbiome data as the dependent variable (Y) and corresponding exposome PCs as the independent variable (X). The R2 value was extracted to represent the exposome's contribution to microbiome data. The same method was applied to evaluate the dietary effect on the microbiome from four body sites.

Seasonal effects on microbiome

Z-score normalized microbial data or microbial diversity was systematically analyzed using Generalized Additive Mixed Models (GAMMs).²⁷⁸ For each genus of interest, the model was formulated as:

$$\text{genera/diversity} \sim \text{IRIS} + s(\text{Time}, \text{bs} = "cc") + (1|\text{Subject_ID}), \text{knots} = \text{list}(\text{TimeOfYear} = c(0, 366))$$

In this model, the response variable 'genera' represents the z-score normalized microbial relative abundance. The fixed effects components include the status of insulin sensitivity (IRIS) and a cyclic cubic spline smoother for the Time variable, encapsulating potential cyclical patterns across the year (from 0 to 366). The term $(1|\text{Subject_ID})$ includes a random intercept for each subject, to account for within-subject correlation.

The model was fitted using the Restricted Maximum Likelihood (REML) method for robust estimation of smoothing parameters in a complex and unbalanced design and incorporated the use of 'lmeControl' function from the 'nlme' package in R to handle the optimization process of the mixed-effects models. This was conducted by specifying 'optim' as the optimizer for the model fit.

The resulting model provides insight into the temporal dynamics of gene expression and its relationship with insulin sensitivity status (IRIS), considering the random effects associated with each subject. The graphical representation of these models for each genus and p value for smooth terms were saved for further exploration.

The effects of infection on microbiome

The analysis of the effects of infection on the microbiome involved genera that were significantly altered during infection periods. The methodology implemented was informed by a previous method for estimating infection processes based on self-reported symptoms.⁷⁰

The infection status was classified into longitudinal categories: pre-healthy (-H) state, event early (EE) state, event late (EL) state, recovery (RE) state, and post-healthy (+H) state. The pre-healthy state comprised the healthy baselines observed within 186 days preceding the onset of the infection event. The EEs state was characterized by visits occurring between day 1 and day 6 of the event. The EL state spanned visits on days 7 to 14 since the onset of the event. The recovery state included visits within the 15–40-day period since the event's inception, and the post-healthy state encompassed visits within the 186 days following the event.

The categorization of these states was designed as a continuous progression from the pre-healthy to post-healthy state, with the average duration of an infection event being 88 days. 58 infection events were detected among 32 participants (IS: 7 participants, IR:12 participants, Unknown:13 participants) in our study. Each event was assigned a unique identification consisting of the subject ID and the event number. The progression of infection states within an event was tracked in the order of pre-healthy, event early, event late, recovery, and post-healthy.

In order to assess the effects of these infection states and insulin sensitivity status on microbiome genera, GAMM was constructed:

$$\text{genera} \sim \text{IRIS} + s(\text{Infection_status}, \text{bs} = "cc", k = 5) + (1|\text{event})$$

In this model, 'genera' represents the z-score normalized microbial relative abundance, IRIS indicates the insulin sensitivity status of each participant, and 'Infection_status' is a smoothing function of the longitudinal infection states with cyclic cubic regression splines. The term $(1|\text{event})$ is a random intercept for each infection event.

For the evenness changes during infection among insulin resistant (IR) and insulin sensitive (IS) individuals, the model was reformulated as follows:

$$\text{evenness} \sim s(\text{Infection_status}, \text{bs} = "cc", k = 5) + (1|\text{event})$$

In this adjusted model, 'evenness' denotes the outcome variable, specifically the Subject ID based Z-score transformed Pielou's evenness measure of the microbiome sample, indicating the diversity of the microbial community. The remaining components of the model and their interpretations align with the previously described model.